5-2024

(Virtual) Space: the Final Frontier – Virtual-Reality-based Identification of Nearby, Young Stars in Gaia Data

Ryan W. Butler
rwb5439@rit.edu

(Virtual) Space: the Final Frontier – Virtual-Reality-based Identification of Nearby, Young Stars in Gaia Data

M.S. *Master of Science*

in Astrophysical Sciences and Technology

Ryan W. Butler

School of Physics and Astronomy

Rochester Institute of Technology

Rochester, New York

May 2024

College of Science
Astrophysical Sciences and Technology

CERTIFICATE OF APPROVAL

MASTER DEGREE Thesis

The Master's. Degree Thesis of Ryan Butler has been examined and approved by the thesis committee as satisfactory for the dissertation requirement for the Master of Science degree in Astrophysical Sciences and Technology.

____
Dr. Joel Kastner, Thesis Advisor

____
Dr. Jason Nordhaus, Committee Member

____
Dr. Michael Zemcov, Committee Member

Date ______________________________

(Virtual) Space: the Final Frontier –Virtual-Reality-based Identification of Nearby, Young Stars in Gaia Data

By

Ryan Butler

A Thesis Submitted in Partial Fulfillment of the Requirements for the Degree of Master of Science. in Astrophysical Sciences & Technology

School of Physics and Astronomy
College of Science
Rochester Institute of Technology
Rochester, NY

May 2024

Approved by:____
Andrew Robinson, Ph.D Date
Director, Astrophysical Sciences and Technology

Abstract

Nearby Young Moving Groups (NYMGSs) are loose kinematic associations of young (<150 Myr) stars in the solar neighborhood (distance $\leq$ 140pc). These groups offer an excellent testbed for the study of pre-main sequence stellar evolution, protoplanetary and evolved disks, and recently formed (or forming) extrasolar systems. To further inform studies of these systems, we can expand the known membership of these NYMGs using the multi-dimensional spatial, kinematic, and photometric data from the Gaia mission. Using a new virtual reality tool known as StarGateVR, we search Gaia Data Release 3 for new candidates of 8 NYMGs and identify $\sim$ 370 such candidates among 7 of the NYMGs investigated. We identify one probable disk-hosting candidate of interest, 2MASS J15460752-6258042, and reassess its age. Finally, the NYMGs are probed for any hot white dwarfs, which could indicate the recent demise of massive member stars.

Contents

List of Figures

List of Tables

Chapter 1

Introduction

1.1 Young stars and their disks

The canonical view of star formation [9] posits a multi-stage process that begins in giant clouds of cold molecular gas, which are regions much denser than the surrounding interstellar medium (ISM). The clouds undergo gravitational collapse, resulting in a hot gaseous protostellar core, which forms a disk and accretes material from its environment. This core continues to contract under its own gravitation, converting potential energy into heat and increasing in temperature and pressure. Eventually, stars with enough mass will begin hydrogen burning (fusing hydrogen in their cores), providing a source of pressure that prevents further contraction. The point at which hydrogen burning becomes the dominant force against contraction is known as the zero-age main sequence, and indicates a star has arrived on the main sequence (MS), where it will remain for the bulk of its life.

The period of a star's life between when they have acquired the bulk of their mass from the initial formation cloud and beginning hydrogen burning is known as the pre-main sequence (pre-MS). The amount of time a star exists in the pre-MS phase is determined by its mass. Low mass stars can spend a great deal of time in this stage (an M star has pre MS lifetime of hundreds of millions of years). Intermediate mass stars such as the sun (a G star) have pre-MS lifetimes of tens of millions of years [10]. The most massive stars, O and B types have pre-MS lifetimes of a few thousand years (for the highest mass O stars) to a handful of million years.

Pre-MS stars are unique laboratories for understanding the early evolution of stars and the formation of planetary systems. By virtue of being (relatively) young, some pre-MS stars are observed to host circumstellar disks [11], often identified by an excess of infra-red emission from the host star. In particularly young stars, these can be gas-rich protoplanetary disks, providing the raw material and gas leftover from the stars formation to give rise to planetary systems. As the star evolves, the gaseous component of this is quickly dispersed, however newly formed planetary systems are chaotic environments, and collisions between planetesimals may give rise to evolved, dusty so-called debris disks which are also observed around some pre-MS stars. The study of these protoplanetary and evolved disks is critical to the overall understanding of how solar systems such as our own arise.

1.2 Nearby Young Moving Groups

The majority of pre-MS stars reside in or around star-forming molecular clouds [12]. In some regards this makes their study difficult, as the clouds they form in create observational hurdles at many wavelengths (notably, optical and ultra-violet), limiting the diagnostic toolkit available to astronomers. Fortunately, discoveries in the last quarter century have lead to the understanding that there is a decent sampling of pre-MS stars closer to home.

Since the 1990s, it has been known that there are several loose groups of pre-MS stars moving together within ~ 120 pc of the sun [13]. These have come to be known as Nearby Young Moving Groups (NYMGs), and by virtue of being spatially and kinematically related, as well as having a common origin, members of a given NYMG share important fundamental properties such as age and metallicity. These NYMGs are very tenuously bound, unlike open clusters, and are not generally observed past ~ 150 Myr in age. Formation mechanisms of these groups is an ongoing area of study - many of them are likely associated with the tidal tails of local open clusters [14], and are old enough that little evidence of their birth nebulae remain.

The first NYMG was discovered in the late 1990's on the basis of strong X-ray emission (an indicator of coronala activity, and hence youth [15]) from the star TW Hydrae and several

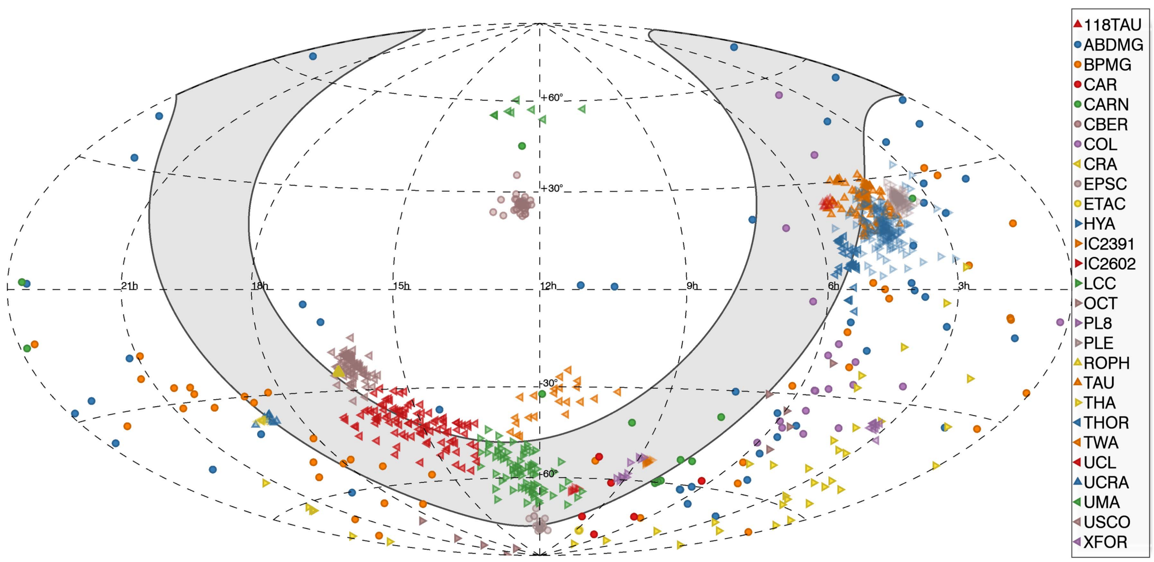

Figure 1.1: Figure 1 from [1] showing all known nearby young moving groups and open clusters current as of its publication in 2018. At least 2 additional groups have been identified since that time [2, 3].

other stars with close physical proximity [16]. Since that discovery, the number of known NYMGs has ballooned to something around 20, although the exact number is still under investigation, and the actual existence of some proposed groups is questionable. Figure 1.1 shows an overview of the NYMGs as of 2018. Because all stars of a given NYMG share the same age, identifying new members is valuable as the age, one of the more difficult properties of a star to ascertain, comes as a given if membership can be verified. As such, stars with other interesting attributes such as circumstellar disks or exoplanets automatically have age determinations for those as well, helping to inform the understanding of the timescales of such systems.

The proximity of NYMGs is of great benefit to the observation of member stars. The aforementioned TW Hydrae provides one of the best resolution observations of a protoplanetary disk to date, due to its convenient inclination and proximity to the sun. NYMG stars also offer by far the best opportunities to directly image exoplanets. To date all directly imaged exoplanets have been around stars within ~150pc of the sun, the bulk of which are NYMG members. This is because pre-MS stars have planets that are still young enough to remain self-luminous in the thermal infrared, and by definition NYMG members tend to be close enough to make such observations possible.

The proximity of NYMGs is also what has made them historically difficult to identify. Because they are so close to the sun, in some cases (such as with the AB Doradus or β Pictoris moving groups) they can cover much of the celestial sphere. This makes them difficult to isolate on position alone in the same way that may be done for something like an open cluster. As such, the best way to obtain new NYMG members is via kinematics. Until the era of widely available 3-Dimensional kinematic data brought about by large radial velocity surveys [17] and Gaia [18], this was difficult. Because of the now much more readily available kinematic and positional data, we have many more avenues to identify candidate members of these NYMGs. Doing so will enhance our knowledge of the structure and composition of these unique systems, further aiding in the study of young stars and solar systems.

Because of their closeness and youth, NYMGs also offer prime targets for identifying recently formed white dwarfs, the stellar remnants left over after certain stars exit the main sequence. NYMGs are young enough that these may be formed from the higher mass (and shortest lived) members, which enter and exit the main sequence very rapidly compared to the majority of lower-mass stars.

1.3 White Dwarfs

Stars of masses $M_* < 8M_\odot$ eventually deplete through fusion the bulk of the hydrogen and helium that they were formed with. In the final stages of these star's nuclear burning portion of life, they tend to eject the majority of their atmosphere through intense stellar winds driven by various pulsations undergone. The brief phase in which a stars atmosphere is being evacuated is known as a planetary nebula [19]. What remains is an inert, hot core known as a white dwarf (WD).

More massive stars tend to evolve on faster timescales than their less massive counterparts. Additional interactions in multiple star systems can also expedite the formation timescales for WDs [20, 21]. WDs which have formed recently are hot (on the order of 100-200 kK) and cool off over time, as such new WDs tend to be brighter than older ones, although all are relatively faint due to their small radii ($R_{WD} \approx R_{\oplus}$).

Because massive stars have a shorter main sequence lifespan, recent WDs which have formed from them can only be found in areas where relatively young stars are present. NYMGs provide an excellent search in this regard, since they are young enough (in many cases too young) to have formed WDs from their most massive initial members which will still be hot, and they are close enough that at least some of these should be detectable. Additionally, if such WDs are detected, it is plausible to probe the surrounding ISM for evidence of the preceding planetary nebulae.

1.4 The Gaia Spacecraft

Gaia is a spacecraft launched by the European Space Agency (ESA) in 2013 with the mission of creating the largest three-dimensional map of the Milky Way galaxy to date by surveying some ~1 billion stars, around 1% of the galaxies stellar population [18]. The primary research purpose of the spacecraft is to conduct astrometry, and as such it measures many related attributes such as position, parallax, proper motion, and radial velocity for sources in which it is viable. Trigonometric parallax, often simply referred to as the parallax, π, or ϖ is the apparent position change of a star seen with respect to the background (usually more distant stars). Because this shift in position is incredibly small it has been difficult to do for a large number of stars until recently. Measuring this parallax with extreme precision for many stars is the primary objective of Gaia. Gaia measures photometry in 3 bandpasses, G (320 nm $\lesssim \lambda \lesssim$ 1100 nm), G_{BP} (320 nm $\lesssim \lambda \lesssim$ 700 nm), and G_{RP} (700 nm $\lesssim \lambda \lesssim$ 1100 nm).

To date ESA has output 3 major public data releases (Data Releases 1, 2, and 3; DR1, DR2, and DR3) from the Gaia mission and one major preliminary release (early Data Release 3). The most recent to this work being DR3 in June 2022, which vastly improved the number of sources with radial velocity measurements [22]. The sheer scale and precision of the Gaia data allows for many new inroads into the search for kinematic and spatial overdensities in stars close to the sun.

1.5 StarGateVR

Virtual reality (VR) is an emergent technology that allows a user to wear a headset with 3D near-eye displays. At present it is largely employed for entertainment purposes, however it has gained some traction in scientific pursuits in recent years [23, 24, 25]. VR offers an underutilized way of engaging with multi-dimensional data, as found in astronomy.

The three-dimensional nature of Gaia data naturally lends itself to a three-dimensional view. VR provides a unique inroad in this regard. To date there have been several tools which have successfully applied Gaia data to VR systems [26, 27, 28]. While these tools provide useful visualizations, they lack some of the data analysis capability of desktop based applications (e.g. TOPCAT [29]) or require attachment to a desktop computer to run.

Our collaboration, particularly Immersive Science LLC, has created a tool known as StarGateVR (SGVR) that successfully overcomes the aforementioned hurdles. SGVR allows the user to view Gaia data on any three axes chosen, provided the data has been pulled from the Gaia archive. It is also of note that the tool naturally renders the data into the intuitive 3-dimensional heliocentric XYZ space for position and likewise UVW for kinematic information, when available. In addition to viewing Gaia data in three-dimensions, SGVR allows the user to select data for further study using a tool in the program known as a "gate", an adjustable ellipsoid which may be dragged through the star field to highlight (known as "gating") sources of interest, as seen in figure 1.2. Sources gated in one set of axes remain highlighted when the axes are changed. In this manner one may observe a star or group of stars in many different ways. The gating aspect of SGVR adds a unique analytical quality to the program not currently seen in other Gaia oriented VR tools.

In this work we apply the StarGateVR tool to the task of identifying NYMG candidate members from field stars in the Gaia DR3 data. We additionally estimate physical properties of these candidate member stars via spectral energy distribution fitting, and in doing so check for evidence of circumstellar disks. The StarGateVR tool is also used to attempt a search of recently formed white-dwarf stars amongst the NYMGs considered in this work.

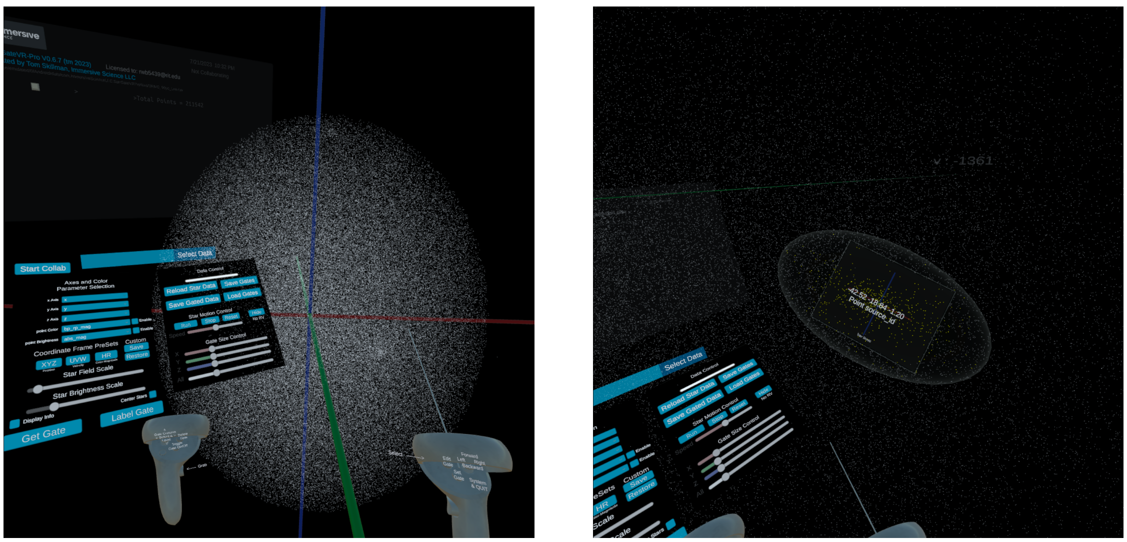

Figure 1.2: Screenshots current to StarGateVR version 0.6.7. On the left, one can see a standard user view in the program, including many prominent user interface elements in the foreground such as the controllers and control panel. A three-dimensional rendered Gaia query is visible in the background. On the right panel the gating ellipsoid is shown prominently, with stars of the Hyades cluster in kinematic space highlighted in yellow.

Chapter 2

New Candidate Members of 7 NYMGs

There exists something of a Catch-22 in the world of NYMG membership. To identify new group members one must fully understand the spatial and kinematic extent of these NYMGs, however to fully understand the morphologies of such groups membership must be well constrained. In this work we approach the membership issue using what is already known about the spatial and kinematic positioning of NYMGs to identify new candidate members.

2.1 Overview of NYMGs Searched for New Candidates

While there exists an ever-changing list of NYMGs under observation, few have well constrained memberships. Perhaps the most complete understanding of NYMG today comes from the first, and particularly well studied, young TW Hydrae Association (TWA) discussed in section 1.2. Other well studied groups include the β Pictoris Moving Group (βPMG or BPMG), the AB Doradus Moving Group (ABDMG), and the Carina, Columba, and Tucana-Horologium Associations (CAR, COL, THA). More recently identified associations, such as the Argus Association (ARG) and 32 Orionis Group (THOR) have also had known membership bolstered within the last decade.

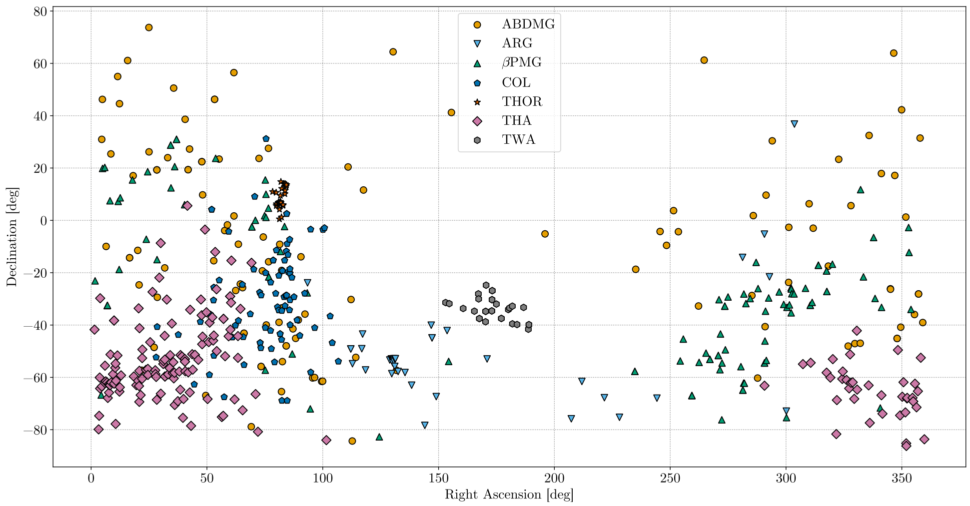

Figure 2.1: Right ascension and declination plot of all bona fide members considered in this work as determined by [4].

2.1.1 Established Memberships

The last several years have seen an increased use in machine-learning methods to tackle data in astronomy [30]. Applications of machine learning to NYMG membership have yielded lists of high-probability group members based on spatio-kinematics in addition to age determinations notably in Lee & Song 2019 [4], hence referred to as Lee+19. For the purpose of this work we consider the bona fide members from Lee+19 to compose the 8 aforementioned NYMGs investigated. A positional plot of the Lee+19 members is given in figure 2.1.

2.2 Membership selection

2.2.1 Gaia Search Criteria

Much of the prior work on membership for these NYMGs was conducted using spatial and kinematic data from Gaia Data Release 2 (DR2) or the later early Data Release 3 (eDR3). We conduct this work using the most recent full data release, Data Release 3 (DR3). Of particular importance is that DR3 contains radial velocities of some 33,812,183 stars, whereas eDR3 and DR2 only contain radial velocities for 7,224,631 stars [31]. This allows us to find many previously unnoticed NYMG candidates because they simply lacked the three-dimensional velocity information to be identified in previous data releases.

The initial search of stars was pulled from the Gaia archive, and encompasses a sphere of stars around the sun with parallax $\varpi > 7.1428571$, corresponding to a distance of 140pc. In theory, NYMGs should exist $\leq$ 100pc from the sun, however in practice several of the groups extend well beyond that distance, so 140pc is taken to allow for maximum candidate consideration. These stars are further filtered on the basis of parallax errors. There are two sources of parallax error considered in this filtering of DR3 data: astrometric excess noise, ϵ_i, and the parallax over error, $\frac{\varpi}{\sigma_\varpi}$. ϵ_i measures the disagreement between observations and astrometric models of a given source, given as an angle. We implement a check of $\epsilon_i \leq 2$ to ensure sources in our selection are astrometrically well behaved. $\frac{\varpi}{\sigma_\varpi}$ considers the measured parallax with respect to its standard error. We additionally check that $\frac{\varpi}{\sigma_\varpi} \geq 20$. This insures that sources with parallax errors > 5%, and hence imprecise three-dimensional positions, are not considered. The resultant cut leaves a sphere of 736,175 well behaved stars out to a distance of 140pc.

2.2.2 StarGateVR Filtering

2.2.2.1 Spatial and Kinematic Filters

Gaia provides precise RA, DEC, and parallax ϖ values for all stars in the sample. StarGateVR, when given a dataset with such values, automatically computes a heliocentric map of the stars positions, known as XYZ space, using code adapted from [32]. In this coordinate system, the X-axis indicates the direction from the sun to the galactic center, the Y-axis is perpendicular to the X-axis along the direction of solar motion through the galaxy, and the Z-axis is perpendicular to both. To maintain a right-handed coordinate system, StarGateVR maintains positive X values in the direction opposite the galactic center. As the system is heliocentric, the sun is located at coordinate (0,0,0).

Gaia likewise provides precise 2-D motion on the sky, known as proper motion (PM), for all stars in the sample. The Gaia proper motion is given as the linear change measured in milliarcseconds in both right ascension and declination per year. The third dimension of a star's motion, that in the radial line of sight (hence known as radial velocity; RV) is much more difficult to ascertain. RVs are generally obtained using Doppler shift, measuring the deviation of an observed spectral line from its expected "rest" position. The Gaia mission is equipped with a dedicated Radial Velocity Spectrometer, allowing it to acquire radial velocity measurements for stars with Gaia G-band magnitude < 14 [33]. Nearly half of the $\sim 700{,}000$ stars in the initial sample lack RV measurements. For those stars which do have measured RVs, a 3-D kinematic analog to XYZ space may be defined, known as UVW space. In this system, U is velocity along the X-axis, V is velocity along the Y-axis, and W is velocity along the Z-axis.

Stars which exhibit similar UVW values implicitly have similar motion throughout the galaxy. This forms the co-moving component of NYMGs. Stars may be co-moving even if they do not occupy a tight locus in XYZ space, but XYZ positions may still indicate a spatial coordination among group members. Leveraging this, we implement a multi-stage filtering process in StarGateVR to identify candidate stars for each NYMG considered.

In addition to the initial 140pc sphere of stars pulled from Gaia DR3, a list of bona fide members of each NYMG determined by [4] is also visualized in SGVR. These bona-fide members serve as "guideposts" for filtering the Gaia DR3 data. For each group, the ellipsoidal gating tool was adjusted and used to select all Gaia DR3 sources that occupied roughly the same spatial positions as the Lee+19 members. A subsequent gate was placed in UVW space, insuring that selected stars occupy not only the spatial region of known group members, but also share similar 3-D kinematics.

2.2.2.2 Color-Magnitude Diagram Filter

The photometric measurements of Gaia allow for the creation of Color-Magnitude Diagrams (CMDs), proxies for the familiar Hertzprung-Russel diagram. Stars of various masses but identical age form distinct tracks on CMDs, known as isochrones. In this way, plotting CMDs

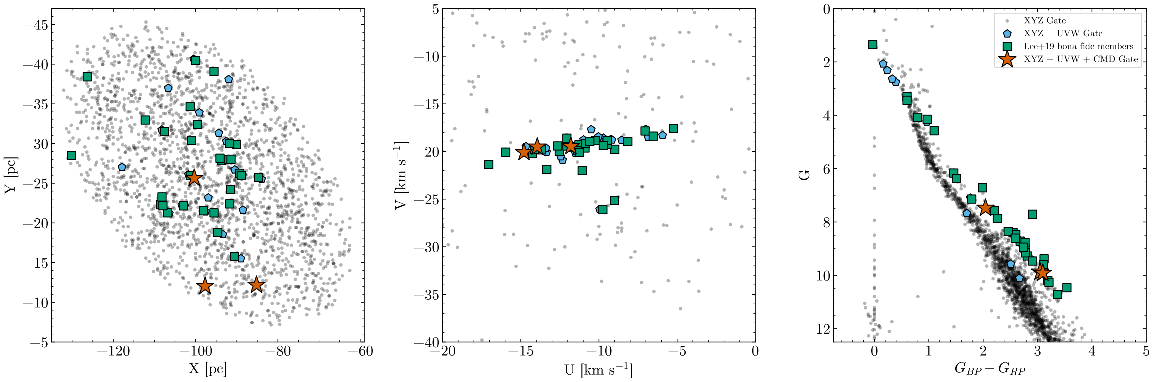

Figure 2.2: Plot illustrating the result of each "gate" in StarGateVR, in addition to showing the bona fide membership used as guides. Note that most if not all bona fide members have Gaia DR3 counterparts which can give an illusion of double-counting on the plots. For simplicity we have shown only a 2-dimensional slice of each gate. The target group in this example is the 32 Orionis group.

of the LEE+19 bona-fide members generates traceable isochrones on the CMDs in SGVR. Using the gating tool in the program, a gate is drawn along the bona-fide members on the CMD, creating a roughcast isochronal filter on all candidate members. Thus, candidate stars of similar CMD positions, kinematics, and spatial locations are identified for all NYMGs. Figure 2.2 shows the sequential results of this gating process on the 32 Orionis group.

2.3 New Candidate Members

The SGVR analysis allowed us to identify a total of 1075 stars between the eight NYMGs. We query the SIMBAD [34] astronomical database for all stars in the sample by Gaia DR3 ID, noting any prior group attribution either in posted literature of the source or publication ingested into the VizieR database [35]. We warn some caution here as literature which has not been submitted to these databases will not be represented in this search. We find that of our SGVR filtered sample, 698 have obvious prior NYMG membership attributions. The remaining 376 candidates lack obvious membership attribution or appear in a different NYMG than identified in our filtering. We do caution that there may exist cases where membership attribution was not ingested into SIMBAD. These are dubbed "new candidates" for the purpose

Table 2.1: Number of Recovered Candidates for Each NYMG. New Candidates Indicate Those Which Were Not Identified in Literature

Group	Total Candidates	New Candidates
ABDMG	322	144
ARG	103	62
BPMG	202	46
CAR	125	64
COL	168	50
THOR	23	3
THA	118	7
TWA	14	0
Total	1075	376

of this work. A dedicated young star database (mocaDB) is due to come online later this year that will likely elucidate prior attribution to some of this sample, particularly for literature which was not input to the SIMBAD/VizieR databases. We report the entirety of these new candidates in table A.1.

Seven of the eight investigated NYMGs appear in the pool of new candidates. The number of new candidates found by group is largely correlated to the group's known size, with the well populated AB Doradus moving group (ABDMG) yielding the most new candidates, and the well studied, low population TW Hydrae Association yielding none.

Of some interest is the location of new candidates in positional and kinematic space. Figure 2.3 displays the XY, XZ, YZ, UV, UW, and VW positions of each newly identified candidate star. ABDMG occupies the largest overall spatial extent, covering a range of around 100 pc in the X direction, and a slightly larger range of $\sim$ 130 pc in Y, and a negligibly smaller range of 90 pc in the Z direction. This is likely a feature of both the ABDMGs statistically larger sampling than that of the other observed NYMGs and more evolved age [36]. The other groups tend to occupy more constrained spatial bounds. In comparison to the positional locations of new candidates, the kinematics are much more constrained and less intermixed between groups, with the noted exception of Carina, Columba, and the Tucana-Horologium association. Although these groups are somewhat distinct in XYZ locations, they exhibit a general overlap in UVW space. Because of this general kinematic overlap as well as similar

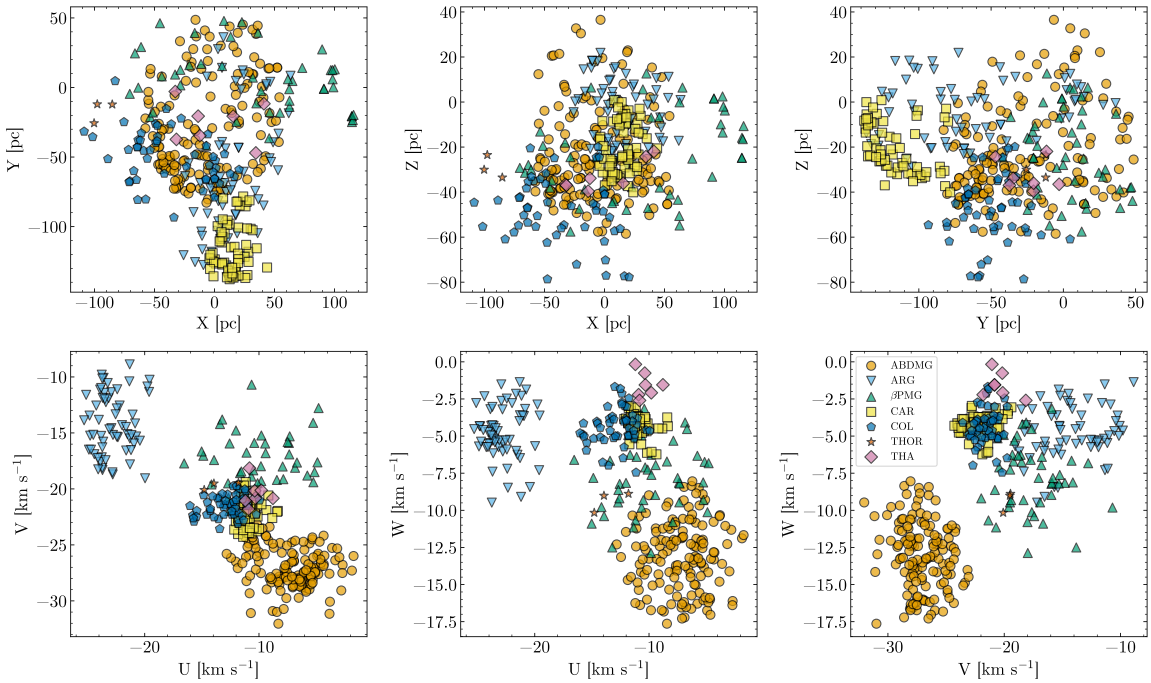

Figure 2.3: Plot of heliocentric spatial and kinematic positions of the new candidate members for each NYMG considered in this work (see table 2.1).

isochronal ages (figure 2.4), these groups, along with the nearby young open cluster χ^1 Fornacis (not considered in this work) have recently been dubbed part of a larger "Austral Complex" [37], although the entire interplay of these groups remains the subject of ongoing research, hence the necessity to better refine and understand the memberships.

2.4 Comparison to BANYAN Σ Membership Probabilities

The processes of converting "candidate" group members to "bona fide member" is a resource intensive process, usually relying on the 6-D spatial-kinematics of the candidate, in addition to independent signs of youth such as strong coronal X-ray emissions, a notable Li 670.7 nm absorption line where applicable, infrared or ulta-violet excess, and isochronal modeling to verify that the candidate matches the full spatial, kinematic, and temporal properties of the NYMG in question. In the event a large list of candidates is generated, as in this work, it is beneficial to compare the candidates to membership models prior to undertaking a full vetting

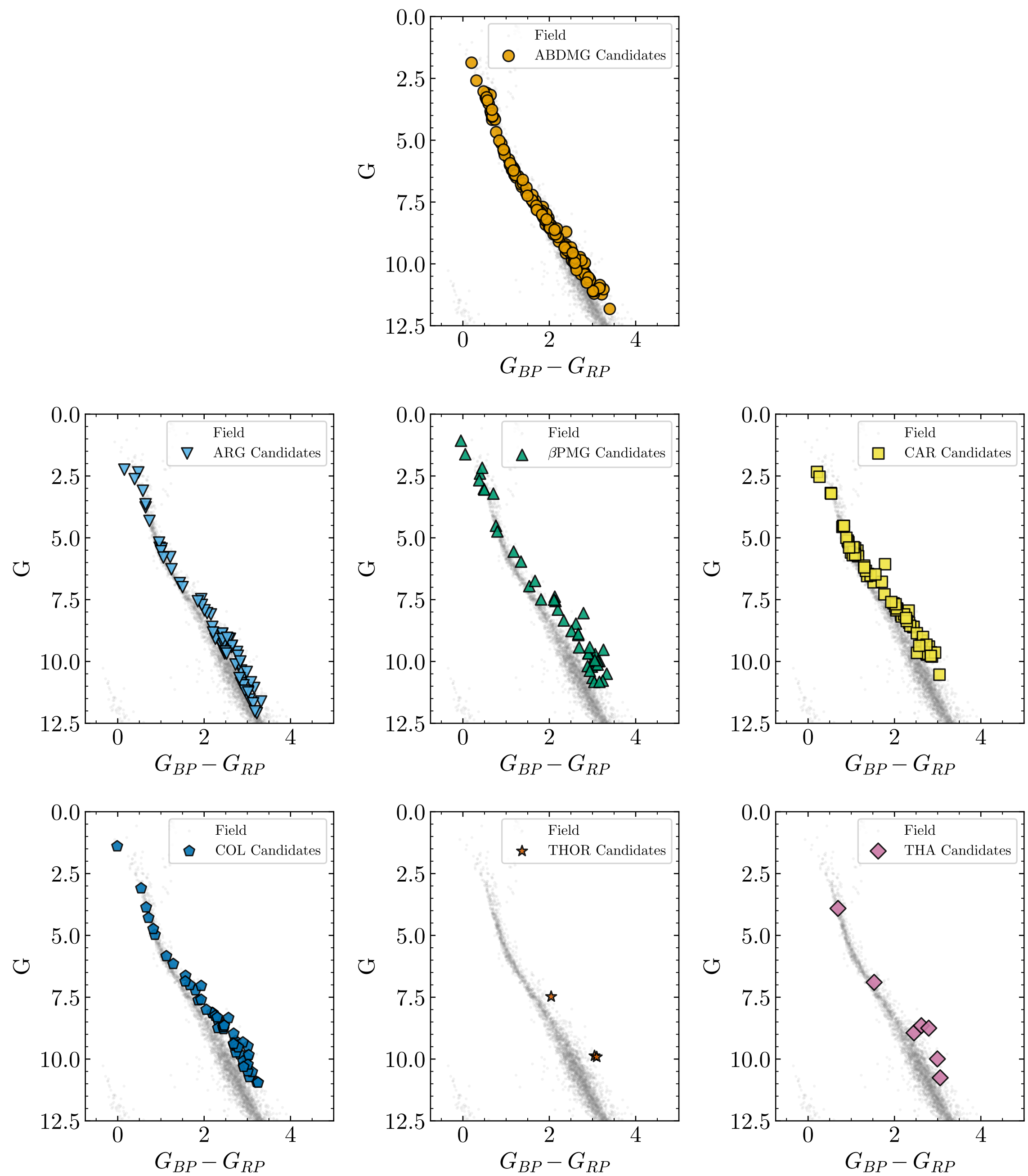

Figure 2.4: Gaia Color-Magnitude Diagrams comprised of new candidates for the 7 NYMGs which yield them in this work. The field stars shown are a randomly selected 12% of stars within 50 pc of the sun.

process.

One such model is BANYAN Σ [1], a bayesian statistical tool which uses the 6-D spatio-kinematics of a star to assess its probability of membership in 29 of the nearest known NYMGs and open clusters. All 7 of the candidate-yielding NYMGs observed in this work have been modelled by the BANYAN Σ tool, although the Argus association is a more recent addition [2]. BANYAN Σ creates its models based on small lists of established members for each group and cluster, and uses ellipsoidal models for both the positional and kinematic extent of groups. The version of the tool used in this analysis does not account for CMD positioning. As such, candidates that return low or even zero probabilities with the tool should not be discarded, as the true morphologies of these groups is still not fully understood. If groups have non-ellipsoidal shapes such as filaments or fans across any space investigated, the tool will not properly model that behavior. With that in mind, a high BANYAN Σ probability for a candidate is a good check that the membership selection process is sound.

All new candidates were run through the BANYAN Σ tool with their full spatial and kinematic values input, along with associated uncertainties. Fig 2.5 provides positional plot of all candidates with color-coding to indicate final calculated probabilities of membership to each respective NYMG. There is a notable distribution on probability outputs by group. Some NYMGs, particularly the Argus association, AB Doradus moving group, and the Tucana-Horologium association yield many high-probability candidates. Others such as the β Pic moving group and the Carina and Columba associations yield a much lower number of high-probability candidate members. Because all candidates are selected with similar CMD placement in addition to XYZ and UVW location, this is not particularly concerning. The interplay between using statistical tools such as BANYAN Σ to identify NYMG candidates and needing to vet NYMG candidates to inform such statistical models provides further motivation for seeking to verify candidates independently, resource intensive as it may be. That said BANYAN Σ provides a useful indicator of which stars may be worth targeting with follow-up studies. If high probability candidates are vetted and found to share properties with known group members, it may indicate that lower probability sources from the candidate pool are

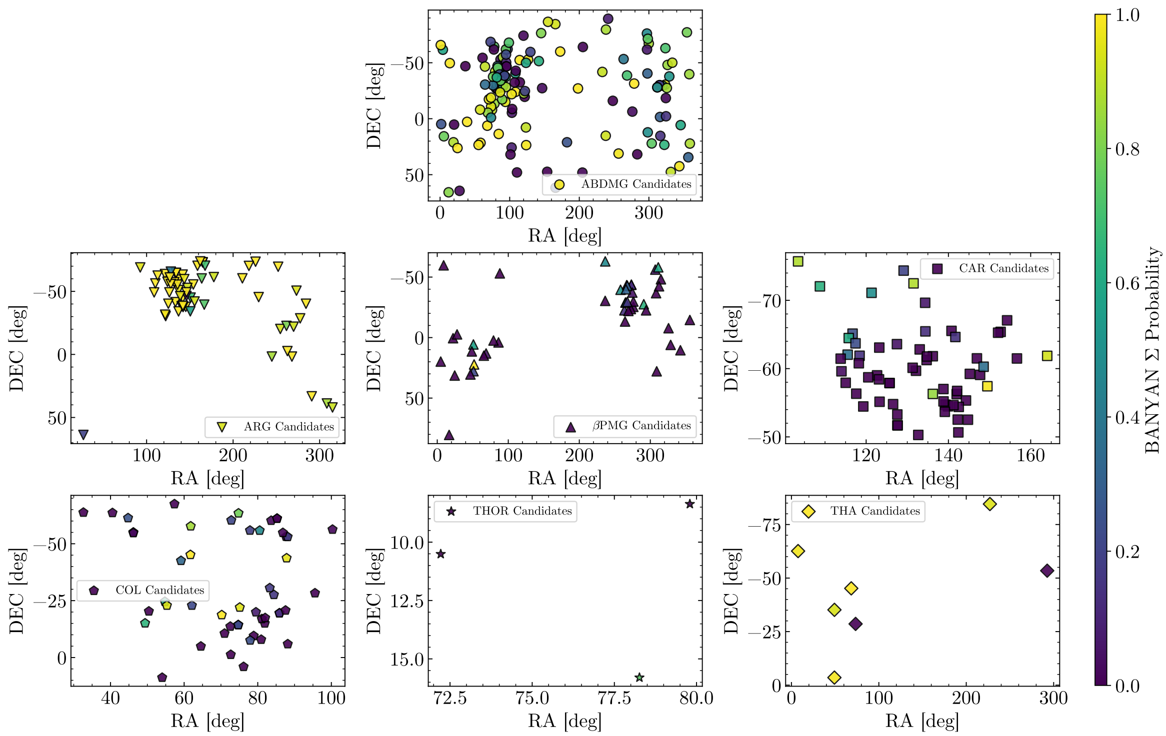

Figure 2.5: Plot of heliocentric spatial and kinematic positions of the new candidate members for each NYMG considered in this work.

also worth investigating.

2.5 Spectral Energy Distributions and Modelling the Physical Properties of New Candidate Stars

By aggregating various individual pass-band photometric measurements we may construct a spectral energy distribution (SED) for each new candidate star in this sample. These SEDs amount to a low resolution spectra of each star, and may be compared with synthetic stellar atmospheric models to estimate physical properties of the star, such as mass, temperature, and radius, that would otherwise prove difficult to ascertain.

We utilize near and far ultraviolet (NUV, FUV) photometry from the Galaxy Evolution Explorer (GALEX) [38], optical photometry from Gaia DR3, and near/mid infrared (IR) photometry from the Two Micron All Sky Survey (2MASS) [39] and the Wide-field Infrared Survey Explorer (WISE) [40] to construct SEDs for all sources. Gaia photometry is present for all sources, 7 sources are found to lack WISE measurements, 6 sources lack 2MASS measurements. GALEX measurements are the hardest to obtain, with 120 sources having NUV measurements and only 47 with FUV. As such, the bulk of candidates only have photometry in the Gaia, 2MASS, and WISE bands. Table 2.3 outlines the wavelength of each photometric band used. Of all bands used, the WISE W4 band has the greatest uncertainty and is vulnerable to contamination from background galaxies and galactic dust. As such, in measurements where the W4 measurement has a large error, it is discarded. In this manner we construct SEDs with as many photometry measurements as possible from the selected catalogues for all candidates. Figure 2.6 shows an example of an SED output with the full queried photometry available. We make use of the Virtual Observatory SED Analyser (VOSA) [41] to compile these SEDs and subsequent model fits.

After SEDs are generated for each candidate using available photometry, a synthetic stellar atmosphere model is fitted to each spectrum. There are a number of such models to choose from, many of which tailor to specific spectral classes or physical regimes of stars. Because our candidates are located along much of the CMD, we opt for the BT-Settl (AGS2009) model

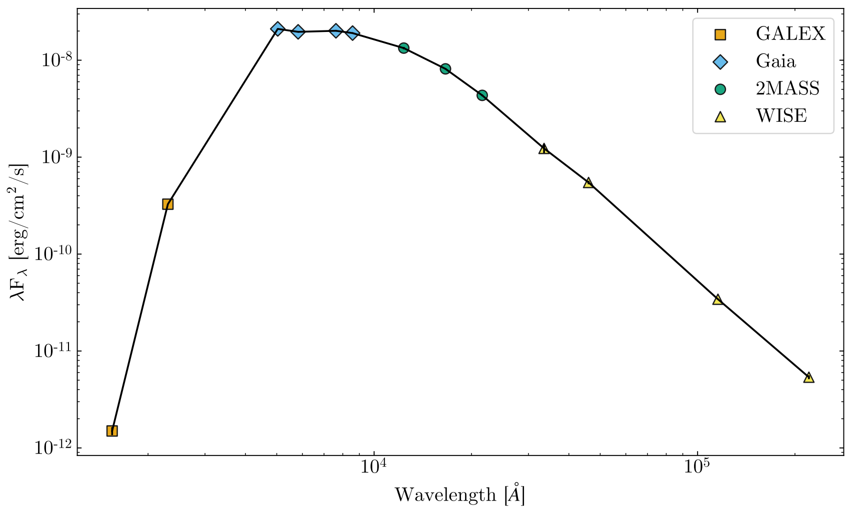

Figure 2.6: Spectral Energy Distribution (SED) composed of GALEX, Gaia, 2MASS, and WISE photometry for candidate Gaia DR3 1192813951126183808. This is a rare example of an SED that contains photometric measurements from all catalogues searched. Error bars are visible but generally smaller than the point size.

grid, which encompasses a wide array of stellar parameters ($400 < T_{eff} < 70{,}000$, $-4 <$ [Fe/H] < 0.5, etc.). VOSA performs a χ^2 fit with the BT-Settl grid and outputs the best 10. For the purpose of this work we opt to select the top ranked "best" fit as given by VOSA, determined as the fit with the minimum χ^2 value. An example of this best fit over a generated SED is shown in figure 2.7. The best fit provides an estimate for the star's temperature, and radius. Using the temperature we also estimate the spectral type of each candidate using the method outlined in [8] for Pre-MS stars, aiding in our growing understanding of the demographics of these NYMGs. The first 10 of these outputs are shown in table 2.2, while the rest are presented in table A.1.

2.6 New Candidates with Infrared-Excess

Circumstellar disks containing dust are known to re-radiate absorbed photons in the mid-to far- IR potion of the spectrum [11]. Consequently, they may appear as larger-than-expected measurements for photometry in that region of the spectrum, particularly in the WISE bands. Identifying stars that host these disks allows for the assessment of an overall disk fraction of

Table 2.2: BT-Settl [7] SED Model Fit Results for First 10 Stars in Sample. Continued in Table A.1. SpT Estimates From [8].

Group	Gaia DR3 ID	RA (deg)	DEC (deg)	Teff (K)	Rad ($R_\odot$)	SpT [8]
ABDMG	4899996487129314688	0.931	-65.78	3500	0.466	M2.5V
ABDMG	2741802191422290176	1.605	4.837	3200	0.371	M4V
ABDMG	4904674604163917696	3.982	-61.631	3200	0.510	M4V
ABDMG	2792563894496829696	5.435	15.727	3200	0.355	M4V
ABDMG	524634348319029888	12.271	65.744	3900	0.440	K9V
ABDMG	4931809967022910976	13.965	-49.64	3000	0.333	M5V
ABDMG	2787564449484699264	19.21	21.052	6700	1.526	F4V
ABDMG	2564275967417666944	20.098	5.252	3800	0.525	M0.5V
ABDMG	292521529517332224	24.997	26.185	4100	0.426	K7V

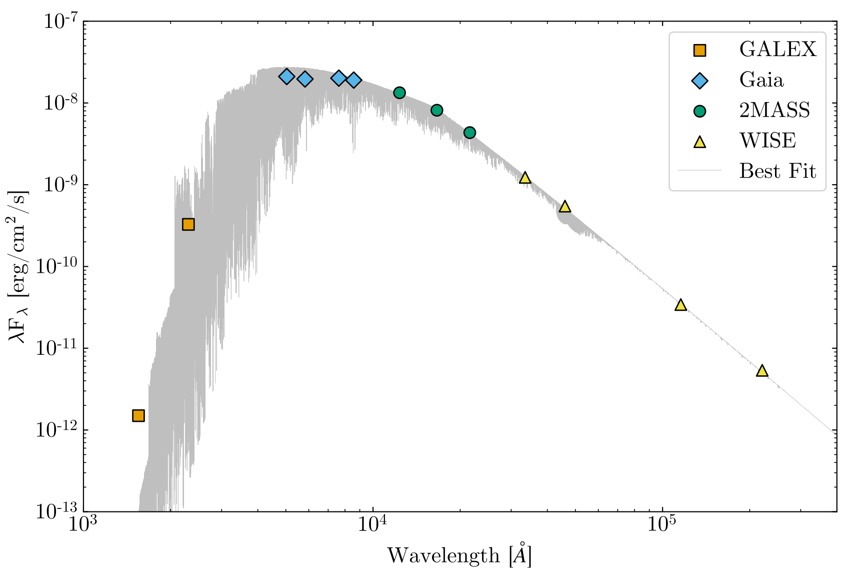

Figure 2.7: SED seen in figure 2.6 with the best fit BT-Settl model overplotted. This particular model corresponds to a star with T_{eff} = 5900K.

stars in a given NYMG. Because the ages of NYMGs are constrained, this contributes to the overall understanding of the lifespans of circumstellar disks both overall and among differing spectral types. VOSA issues a flag on any source that it detects such an excess in during SED generation. Circumstellar disks are not the only possible cause of IR excess however, as any foreground or background dust, in addition to background galaxies, may also lead to the unexpectedly large IR measurements. As noted previously, the WISE W4 band is particularly sensitive to these types of contamination. Additionally, the presence of a nearby, bright star in the same field may also lead to an excess. For these reasons, it is important to vet each IR-excess displaying candidate.

Of the 376 new candidates for which SEDs were created in section 2.5, 20 are identified as having IR-excess. The majority of these display an excess beginning in the WISE W1 band, with others beginning in longer-wavelength bandpasses. No candidates are identified with obvious excess from the 2MASS measurements. The WISE W1-4 band images were then reviewed for each of the IR-excess sources. Of the 20 sources, we identify only 8 that appear obviously in all WISE frames. The majority of those that do not are found to be binaries, or exhibit obvious dust contamination in the W3 and W4 images which likely lead to the IR excess seen in their SEDs.

Of the 8 candidates which are detected in all WISE bands, we note that at least two, Gaia DR3 4900997562402606208, and Gaia DR3 5298425111243573376 are binary systems, which may contribute to the IR excess. 4 others, Gaia DR3 5826466047245658240, Gaia DR3 5487374844438857728, Gaia DR3 123185851098826880, and Gaia DR3 4066318531598567424 are already known disk-hosts [42, 43, 44]. The final two sources, Gaia DR3 5301812603489357440 and Gaia DR3 5275773488076705024 have no noted literature references to disks.

Table 2.3: Approximate λ_{eff} Value For Each Bandpass Used in SED Generation

GALEX		Gaia				2MASS			WISE			
FUV	NUV	G_{RP}	G	G_{BP}	G_{RVS}	J	H	K_S	W1	W2	W3	W4
nm	nm	nm	nm	nm	nm	μm	μm	μm	μm	μm	μm	μm
152.8	231.0	503.6	582.2	762.0	857.8	1.235	1.662	2.159	3.368	4.618	12.082	22.194

Chapter 3

A Peter-Pan Disk Exits Neverland: Reevaluating the Age of Disk-Hosting Star 2MASS J15460752-6258042

Typically, gas-rich protoplanetary disks are battered by the stellar winds of the host star and are expected to dissipate on a timescale of a few Myr [11], while dusty debris disks formed by colliding planetesimals may exist much longer into a star's evolution. Infrequently, a star is identified that displays evidence of hosting a gas-rich disk despite an age older much older than the expected evaporation timescale (> 10 Myr) [45, 46]. Known examples of stars with these long lived gas and dust disks include the ~ 12 Myr binary V4046 Sagittarii [47] and the dusty $\sim 30 - 50$ Myr old RZ Piscium [48]. Because the exact intricacies of disk life-cycles remains an open question, it is important to identify these so called "peter-pan disks" and study them. It is likewise important to accurately assess the ages of these disks, to help paint a complete picture of the overall evolution and properties of these objects.

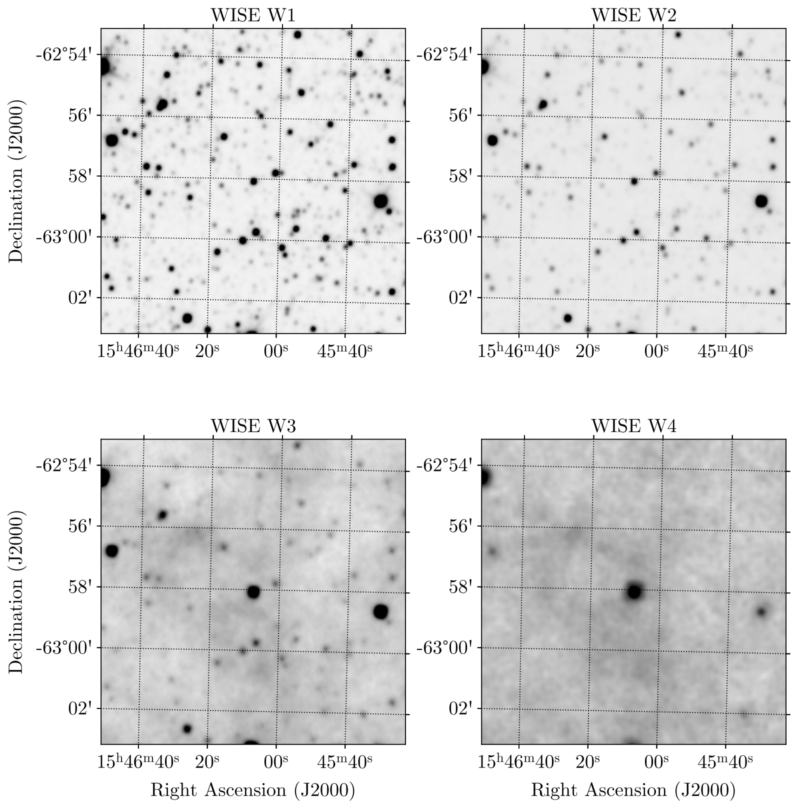

Figure 3.1: WISE W1-4 band images of J1546. Increased IR emission seen in the W3 and W4 images, compared to all other stars in the images, is evidence of the circumstellar disk thought to exist around the star.

3.1 Previous Studies of 2MASS J15460752-6258042

2MASS J15460752-6258042 (identified in the Gaia catalogue as Gaia DR3 5826466047245658240, known hereafter as J1546) is an understudied curiosity amongst circumstellar disk hosting stars. It was initially observed in the infrared by 2MASS and later WISE (figure 3.1). It was identified as an Hα emission line T-Tauri star in 2014 as part of a South African Large Telescope (SALT) spectroscopic follow-up to several Hα sources [49] identified in the AAO/UKST SuperCOSMOS Hα Survey [50], with aims of identifying symbiotic stars.

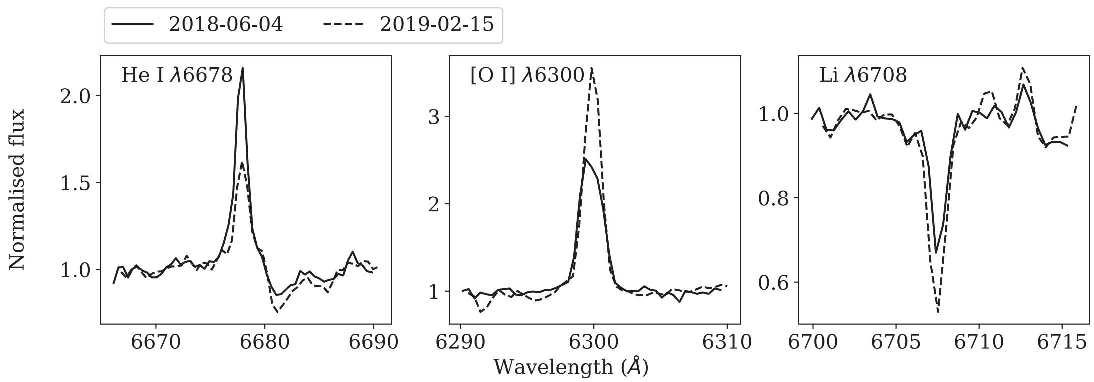

Figure 3.2: Figure 4 from [5] showing the line profiles of He I, [OI], and Li I. The variationm between observations is likely an effect of the ongoing accretion.

A set of spectroscopic observations in 2018 and 2019 further refined the Hα detection, showing an equivalent width in excess of 100 Å in both spectra. Lee+20 [5] (Lee+20 hereafter) also identified other emission lines (Balmer series, HeI, [OI]) in addition to a prominent Li I absorption line at 6708Å. Figure 3.2 shows the spectrum of the notable emission and absorption lines from that work. The behavior seen in the Lee+20 spectra is consistent with other disk-hosting stars, with the Hα strong emission lines supporting this.

Using their measurements, Lee+20 identifies J1546 as a spectral type M5 probable member of the Argus moving group. As Argus has as constrained age [2] of $\sim$ 55 Myr, this gives J1546 the distinct title of oldest mid-M star with an accretion disk identified current to that work.

3.2 StarGateVR Recovery of J1546

Using the processes outlined in sections 2.2.1 and 2.2.2, we recover J1546 as a candidate member for the much younger β Pictoris Moving Group ($\sim$ 20 Myr [51, 52]). As it has not been formally designated a member of any NYMG (with Lee+20 giving probabilities but no bona fide status) the star entered our pool of new candidates for the group. A complete list of the spatial and kinematic Gaia DR3 parameters is given in table 3.1.

Table 3.1: Complete list of spatial and kinematic values from Gaia DR3 used in determining our position and velocity of J1546

RA (deg)	DEC (deg)	ϖ (mas)	σ_{ϖ} (mas)	PMRA (mas yr^{-1})	σ_{PMRA} (mas yr^{-1})	PMDEC (mas yr^{-1})	σ_{PMDEC} (mas yr^{-1})	RV (km s^{-1})	σ_{RV} (km s^{-1})
236.531	-62.968	17.013	0.031	-42.776	0.036	-61.791	0.031	2.526	2.381

3.3 Analysis

3.3.1 Spatio-Kinematics

We find the Gaia DR3 derived spatial and kinematic heliocentric positions paint a confusing picture of group membership for J1546. It is clear in figure 2.3 that J1546 occupies a region of space which cannot be strongly attributed to either group. Despite the muddled position of J1546, the kinematics of the Gaia DR3 measurement indisputably favor a βPMG membership attribution. This is noted with the heavy caveat that the Gaia derived radial velocity is not in good agreement with that determined in Lee+20, and uncertainties are not large enough in either case to reconcile the positions. If this variation in RV over time is real, it may indicate the presence of a punitive companion not detected by Gaia.

A BANYAN Σ analysis of the Gaia DR3 kinematics additionally favors a βPMG membership, attributing it a 46.9% probability. The Argus moving group yields a 0% probability, while the Upper Centaurus Lupus (UCL) association, not considered in this work has a small 3.7% probability. BANYAN Σ also gives a 49.4% probability that J1546 is a field star.

3.3.2 Color-Magnitude Diagram

Figure 3.4 shows that J1546 clearly occupies a transitional region of the CMD between the tracks formed by members of the Argus and β Pic moving groups. This position is further complicated because the disk inclination of J1546 is unknown. An edge-on or similarly obscuring view of the system that will “lower” the stars CMD position cannot be ruled out without further observation. The PARSEC isochrones should be interpreted with some caution as they only represent a solar metallicity regime, and theoretical isochrones have historically struggled to accurately model behavior of late-type pre-MS stars.

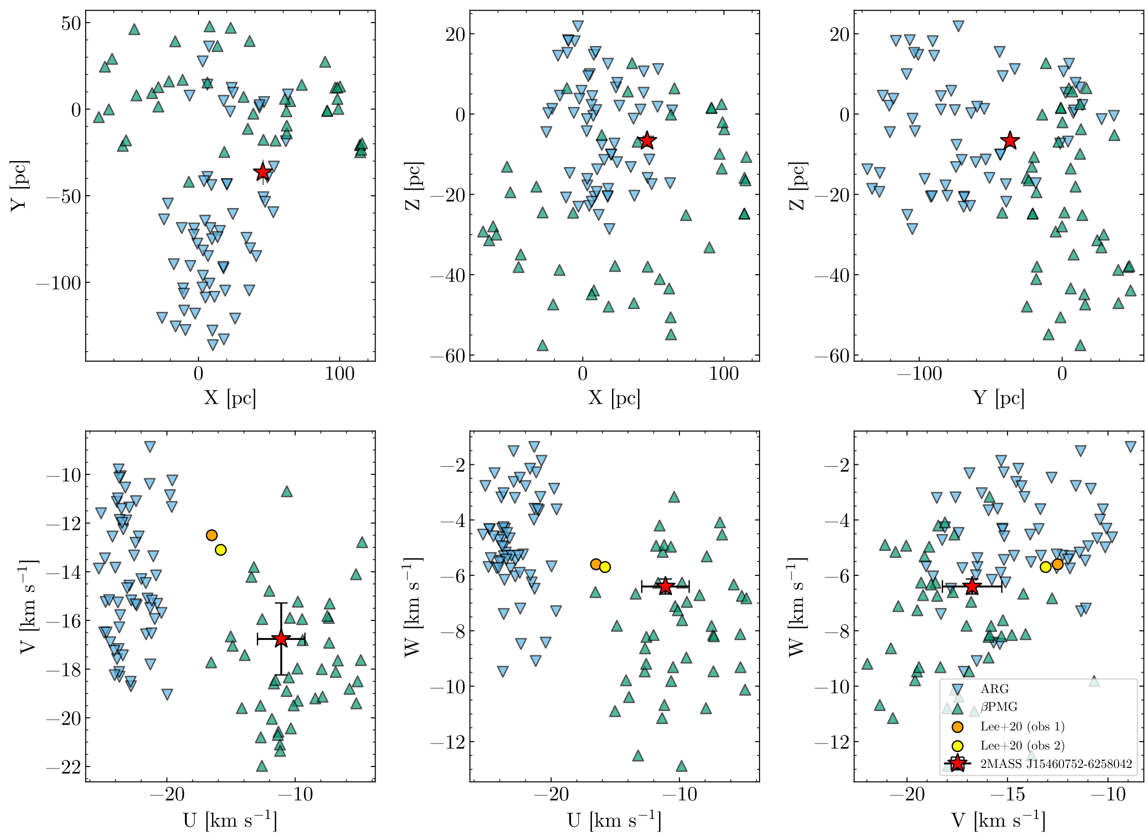

Figure 3.3: Spatial and kinematic positions of J1546 (this work) are shown in red with respect to bona fide members of the Argus and β Pictoris moving groups. Included are the UVW positions for J1546 as found in Lee+20. Error bars are smaller than point size in XYZ.

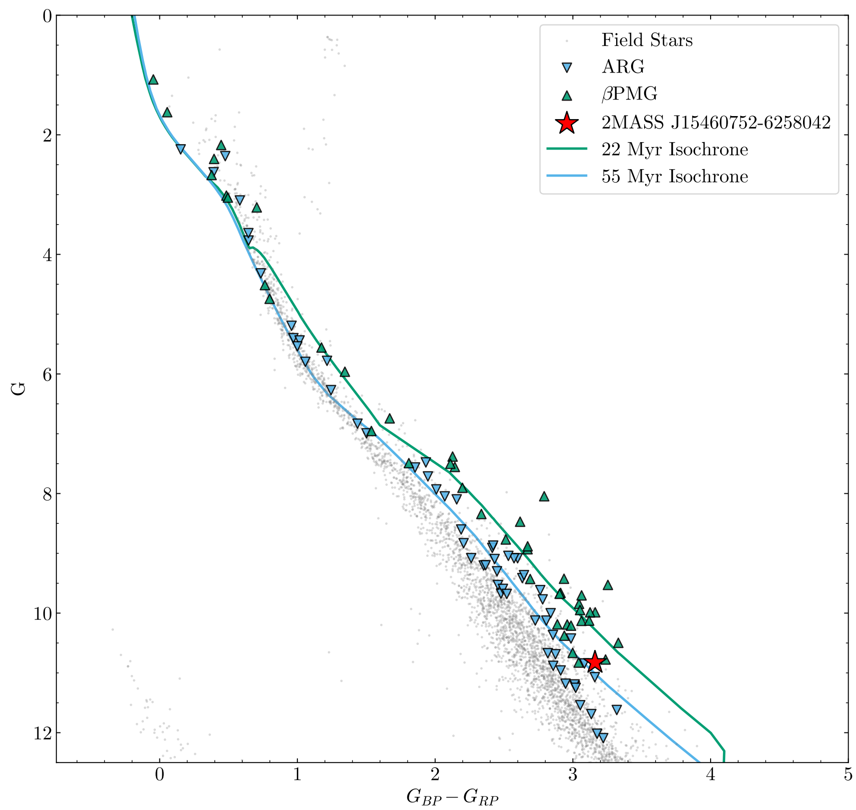

Figure 3.4: Gaia CMD of the bona fide members the Argus and β Pictoris moving groups [4] with the location of J1546 (this work) noted in red. Additionally plotted are theoretical PARSEC isochrones at the approximate ages of the moving groups [6]

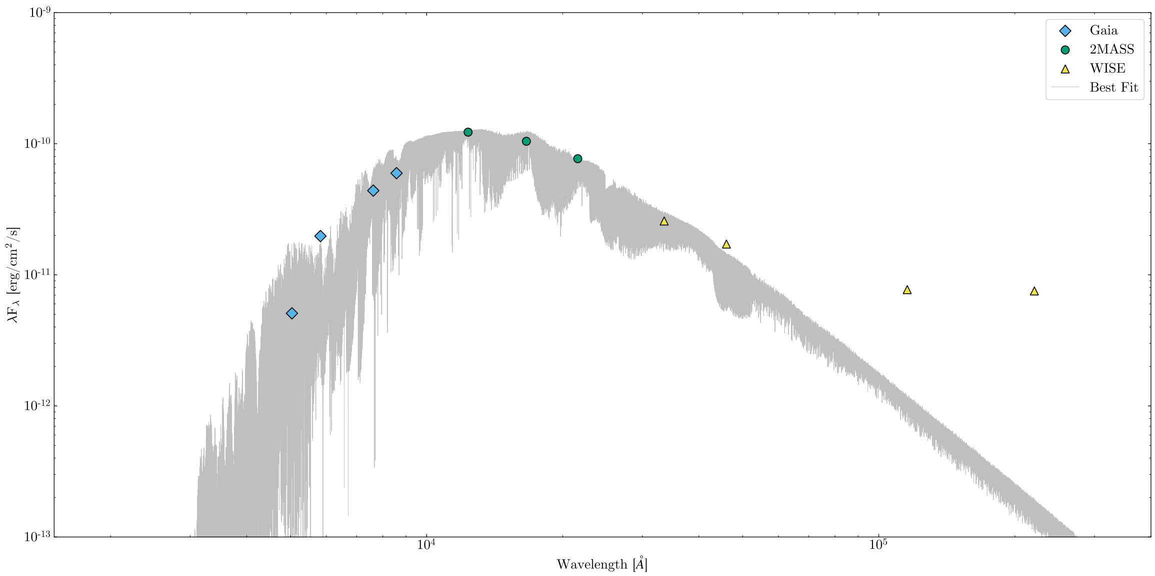

Figure 3.5: Spectral energy distribution (SED) and best BT-Settl model fit for 2MASS J15460752-6258042. The best fit star yields a T_{eff} = 2900 K. Note the extreme deviation of the actual SED from the best fit in the infrared (particularly the WISE W3 and W4 bands), evidence for a circumstellar disk. Errors on photometry are smaller than point sizes, no GALEX data was available for this source and was thus not used in the SED or fit.

3.3.3 Spectral Type

As with all other candidate stars, an SED of J1546 was generated and modeled with the BT-Settl model grid as outlined in section 2.5. The resulting SED and subsequent fit are shown in figure 3.5, with the infrared excess that lead to a further interrogation of this object clearly visible. We find an effective temperature estimate of 2900 K, representative of an M5/M5.5 spectral type per [8]. This is in agreement with Lee+20, which gives an M5 spectral type and similar temperature.

3.4 On The Age of 2MASS J15460752-6258042

It is difficult to assign a NYMG membership to J1546 with high confidence. The spatial coordination, as is too often the case with NYMGs, is not extraordinarily insightful. The Gaia kinematics firmly associate the start with the β Pictoris moving group, a conclusion which is supported by the BANYAN Σ model. This lies in contrast to ground based radial velocities which favor an Argus membership, although those spectra have a slightly lower resolving power than that of Gaia's RVS (R = 7,000 vs. R = 11,500 [33], although Gaia targets a very limited part of the spectrum). The CMD position also lends credence to Argus membership, but the extent of veiling and self-extinction due to system inclination are unknown. We also note that if there is indeed an undetected close companion, this would elevate the CMD position of V1546, putting it closer to the Argus association in actuality.

An additional clue to the age of this object is the Lithium 6708 Å equivalent width (EW). Lithium is rapidly depleted as stars evolve. While this rate depends on many physical parameters of a star, these may be amalgamated to determine (roughly) the expected equivalent widths of the Li 6707 Å line. Lee+20 reports EW measurements for the 6707 Li absorption line (figure 3.2) of 430 and 600 mÅ, which is in line with previous measurements for mid-M stars in βPMG [53, 54, 55]. As they note however, the ongoing accretion may actively replenish Li in the atmosphere of J1546, leading to the different values for the time separated measurements. As such, this again does not yield distinct proof of either group attribution.

Because the group membership of J1546 remains uncertain, we recommend adopting a much wider age range in future discussion about the object, until clarifying observations are undertaken. As such, a liberal age range should be adopted when discussing J1546 between $\sim 20 - 55$ Myr, given current age constraints on both the β Pic moving group and Argus association [56, 2]. Even in the case where this object has an age revision down to the βPMG standard, it still amounts to an unusually long lived accretion disk, worthy of additional study. Follow up observations, particularly high resolution spectra would be beneficial in reaffirming the Hα and other emission line defections indicating accretion. Additional measurements of RV are needed to properly assess the group membership of J1546 and, if the RV variability is real, put constraints on the physical parameters of a thus far unseen companion.

Chapter 4

Searching For White Dwarfs in NYMGs

4.1 Young WDs in the Solar Neighborhood

Identifying young white dwarfs in the solar neighborhood can help answer important questions in regards to the age of nearby young stellar associations and star clusters, and help to verify our understanding of the initial mass function for these systems and the galaxy at large [57]. Typically, these young, massive WDs are identified by association to known groups, particularly the nearest open clusters such as the Hyades (age $\sim 600 - 700$ Myr [58]) and the Pleiades (age ~ 120 Myr [59]). Estimating the WD formation and cooling times also provide a valuable age estimate of these systems independent of other common methods such as the lithium depletion boundary or main-sequence isochrones [60].

In 2018, the ultra-massive WD GD 50 was identified in association with the AB Dor moving group [60] (age ~ 120 Myr [36]). This denotes the first known WD in a NYMG, evolving from a progenitor with an initial mass very close to the 8 $M_{\odot}$ threshold for WD formation. To date, no other NYMG WDs have been identified, and any that will be must have resulted from a similarly massive progenitor or evolve in non-single star systems.

4.2 Search Criteria

As with the initial search of NYMG candidates we utilize a joint approach of data and the StarGateVR tool to identify WDs that may be associated with NYMGs. The initial DR3 sample is the same as that described in section 2.2.1, and once again we utilize the bona fide candidates from [4] in conjunction with those data.

Again using the SGVR tool, we initially select out all stars that share the approximate XYZ with the majority of bona fide members of a given NYMG. Unlike the previous selections however, we cannot utilize the heliocentric kinematic space to refine the search. This is because WDs are very faint, and the majority of those in the Gaia search lack radial velocity measurements. As such, we are limited to considering the 2-dimensional proper motions of the candidates. With SGVR, we select out the subset of stars which match both the XYZ positions and proper motions in the right ascension and declination. We are further inhibited from selecting similar CMD positions to bona fide NYMG members as none of the membership lists utilized contain WD members. As such, we impose a cutoff at $G_{BP} - G_{RP} \leq 0$, where G_{BP} and G_{RP} represent the Gaia blue and red photometric bands respectively, and select all sources of that disposition in the WD portion of the CMD which have also share similar positions and velocities with bona fide NYMG members.

An additional cutoff at $G_{BP} - G_{RP} \leq -0.15$ is applied to the data following the SGVR analysis, noting that GD 50, the WD member of the AB Doradus moving group has an $G_{BP} - G_{RP} \approx -0.5$ and it is unlikely that we will identify any candidates older than that, given that all NYMGs considered in this work are the same age or younger than the AB Dor moving group. It is possible that multiple star systems can yield WDs on an expedited timescale, but it is likely that any WD formed in that manner will be "washed out" by the companion and thus will not enter the WD part of the CMD.

4.3 WD Candidates

After filtering the sample in SGVR, we identify 47 candidate WDs among 6 of the 8 NYMGs considered, with 4 WDs being recovered in 2 NYMGs. No candidates are identified in the TW Hydrae association or the 32 Orinis group. The bulk of these (31) are found in association with the XYZ position and proper motion of the β Pictoris moving group. The β Pic moving group encompasses much of the sky, and consequently have a wide spread presence in proper motion space, as well as in positional space, so this effect is likely an artefact of a large filter rather than a true physical effect. The number of candidates recovered between the other groups is 7, 1, 1, 9, and 1 for the AB Doradus moving group, Argus association, Carina association, Columba association, and Tucana-Horologium association respectively. The aggregate CMD positions for all of the candidates is shown in figure 4.1.

4.4 BANYAN Σ Results

Because we are particularly limited in our set of observational diagnostics (i.e. no Gaia RVs or bona fide WD CMD tracks to trace) the BANYAN Σ tool is particularly insightful. We input all 51 sources. BANYAN Σ will natively query SIMBAD to pull values that are not input by the user if available. In this manner we are able to recover RV values for several of the candidates. BANYAN Σ returned a null NYMG probability for all but 8 candidates. Aside from one star, HZ 14 which is identified both by BANYAN and the literature as a Hyades cluster member [61], the 7 of the remaining sources have BANYAN Σ probabilities exclusively with regard to the Argus association, although all were recovered in association with other NYMGs in SGVR. These stars, their SGVR recovered groups, and their Argus BANYAN Σ probabilities are given in table 4.1. It is noted that BANYAN Σ failed to identify known RVs for any of these sources and thus the probability is based only on position and proper motion. Figures 4.2 and 4.3 show the XYZ and proper motion positions of the BANYAN Σ identified WDs with Argus probability against the bona fide list used in this work.

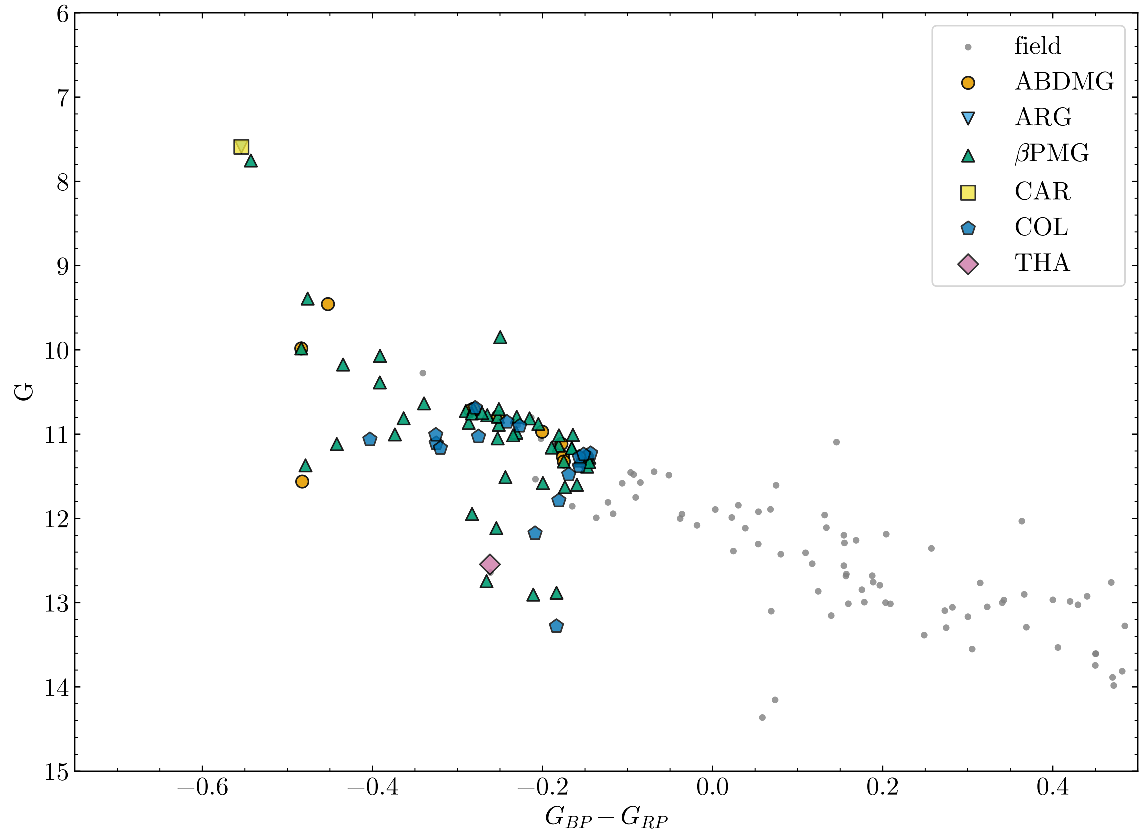

Figure 4.1: SGVR recovered WDs on the Gaia CMD. Field stars are from a randomly selected 12% of the nearest 50 pc. Note that the most recently formed, hottest white dwarf candidates occupy the region left of $G_{BP}-G_{RP} = 0.4$

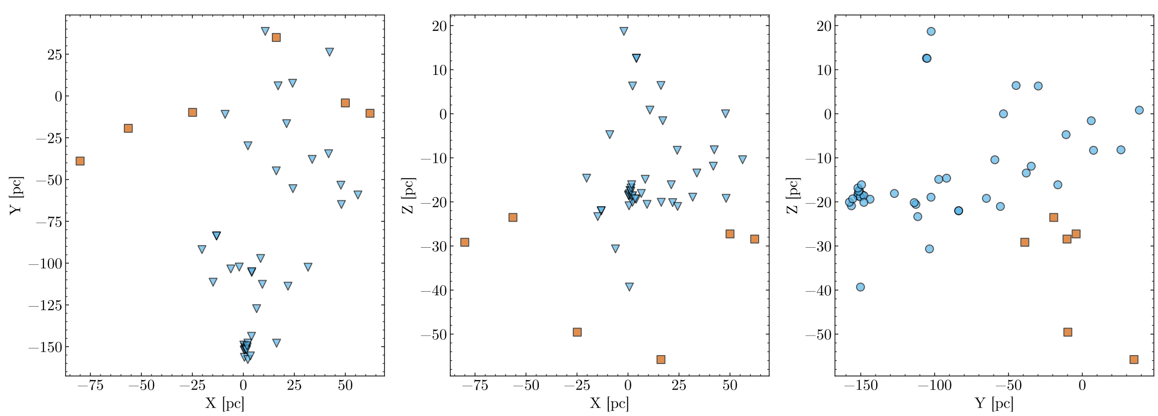

Figure 4.2: 3-D heliocentric positions of both the bona fide membership used as a guide for SGVR filtering and the WD candidates with non-zero BANYAN Σ Argus probabilities. Legend is the same as that in figure 4.3.

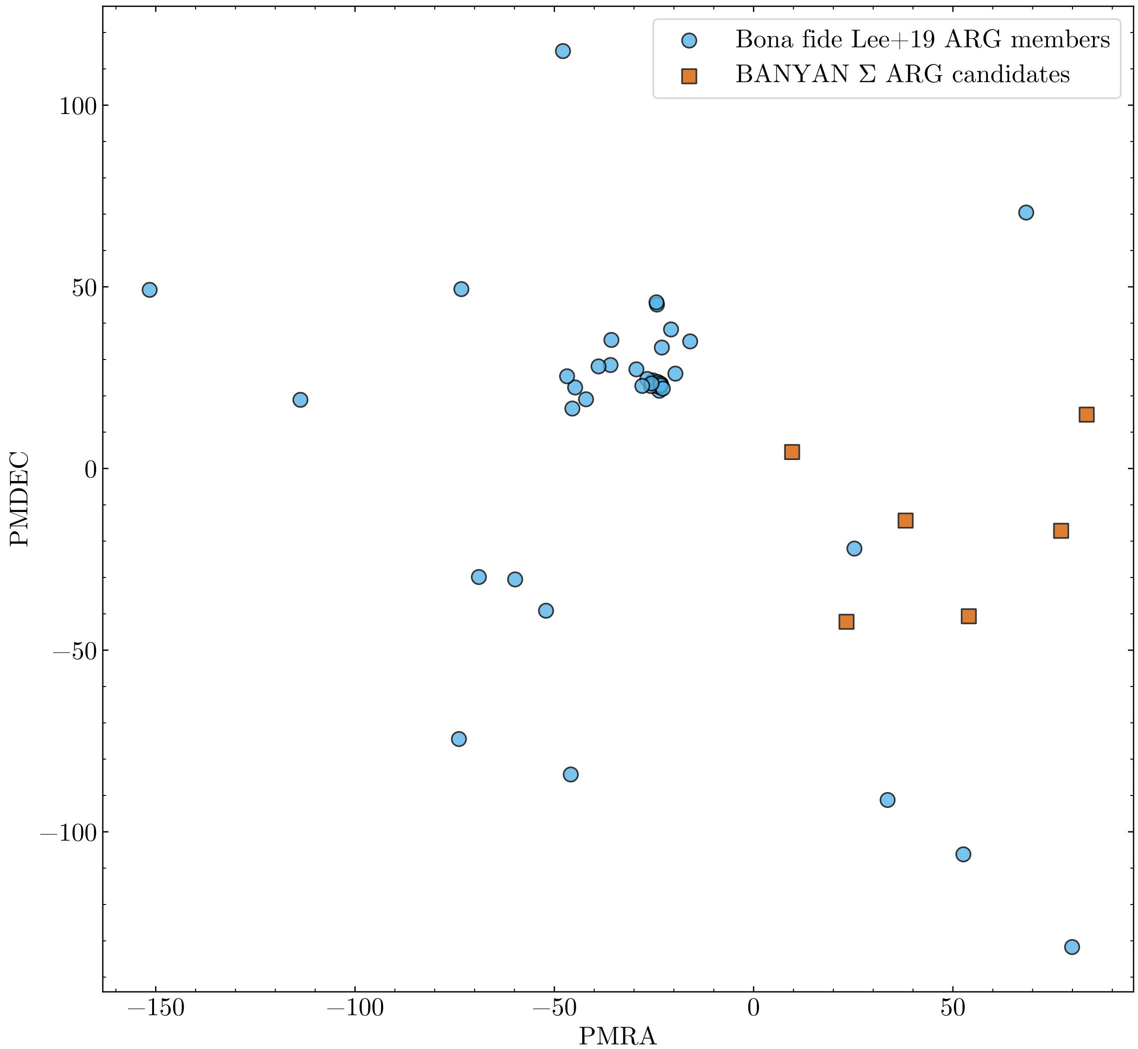

Figure 4.3: Proper motions in the right ascension and declination for both the bona fide membership and the WD candidates with non-zero BANYAN Σ Argus probabilities.

Table 4.1: SGVR Recovered WDs with BANYAN Σ Non-Zero Probability.

Gaia DR3 ID	SGVR Group	BANYAN Σ Group	Probability
6663138531316128640	βPMG	ARG	34
6685137182005209216	βPMG	ARG	0.9
292454841560140032	βPMG	ABDMG	0.2
2611722922108815872	βPMG	ARG	61.4
3216947242193857024	COL	ARG	51.4
3234818257515161856	COL	ARG	62
5129157117202633216	THA	ARG	94.4

4.5 Discussion

It is unlikely that any of the recovered WDs are affiliated with the NYMGs considered in this work, given the extraordinary timescale required for such formation to occur for most stellar mass regimes capable of producing WDs through single-star evolution. At the high end of that regime ($\sim 8M_{\odot}$) the stars have a main-sequence lifetime on the order of 50 Myr, and nearly all of the observed NYMGs are younger than that. The BANYAN Σ derived probabilities of membership to the Argus association among many candidates poses an oddity but should not be outright dismissed, especially for the higher probability sources. The XYZ positions are not extraordinarily distant from those of bona fide members, and proper motion alone may not be a sufficient consideration of the velocity space. Radial velocities are needed for these sources to concretely rule on affiliation with the Argus association, particularly for the high probability candidate (based on position and proper motion) Gaia DR3 5129157117202633216.

Of additional interest is the population of WDs recovered with $\mathrm{G}_{BP} - \mathrm{G}_{RP} \leq -0.4$. Regardless of NYMG association or lack thereof, these represent some of the hottest, most recently formed WDs in the solar neighborhood. This is especially true for the two candidates identified with $\mathrm{G}_{BP} - \mathrm{G}_{RP} \leq -0.5$, one of which is well studied while the other, Gaia DR3 5318772982658411008 is particularly understudied. By ascertaining the formation timescale of these WDs we may be able to probe the surrounding ISM for any evidence of their previous, short-lived planetary nebulae, something interesting irrespective of NYMG membership.

We also note that while this method does not recover droves of WDs in the NYMGs, it may be much more readily applied to more evolved associations of stars, such as nearby open clusters or stellar streams. The incidental recovery of a Hyades WD lends credence to this approach.

Chapter 5

Conclusions

5.1 Summary

In this work we have sought to identify expand the list of known nearby young stars to facilitate future studies of direct imaging studies of exoplanets, and the study of early stellar evolution after the stars have left their molecular clouds. We interrogate 8 NYMGs, the AB Doradus and β Pictoris moving groups, as well as the Argus, Carina, Columba, Tucana-Horologium, TW-Hydrae, and 32 Orionis associations. Using a new virtual reality tool, StarGateVR, we recovered over 1,000 candidate members between those 8 NYMGs, and found some ~ 360 of those to be poorly identified in preexisting literature, not identified at all, or associated with a different group than determined in this work (although this may change with a new young star database coming online in the near future). We find 20 of these candidates exhibit infrared excesses and thus are possible hosts to circumstellar disks, although many of these can be ruled out upon further examination of the WISE images.

One of the identified IR-excess stars, 2MASS J15460752-6258042, has previously been identified as an extraordinarily long lived accreting disk host, given an age of ~ 55 Myr based on prior assigment to the Argus association. Our work calls this age into question, recovering the star in association with the younger (age ~ 20 Myr) β Pictoris moving group, primarily based on Gaia DR3 derived kinematics. We note that further observations of the star must be undertaken to fully constrain its group membership and hence age, and recommend noting a wide age range ($\sim 20-55$ Myr) until this has been done. Regardless of the true age of J1546, evidence does suggest in either case it hosts a long-lived accretion disk and for this reason alone should be considered for future study.

We additionally attempt to use the SGVR to identify possible high-mass, recently formed WDs associated with the NYMGs considered in this work. While we do recover ~ 50 WDs, we note that these candidates lack DR3 radial velocities and thus have been selected on 3-D motion and proper motion, which is not ideal for accurately assessing membership. Additionally, the evolution timescale for even the most massive possible single stars to reach the WD stage is generally longer than the accepted age of groups considered, further adding to the likelihood that these candidates are not associated with any NYMGs in actuality. Despite this, the method for identifying WDs outlined is sound and may be applied to other, perhaps more evolved systems in the solar neighborhood.

5.2 Future Work

Virtual reality has proven to be a powerful tool for working with large sets of multidimensional data such as Gaia, something seen with increasing frequency in astronomy. Increasingly, astronomers have leaned on machine-learning techniques to probe such massive amounts of data. Virtual reality tools such as StarGateVR offer a way to check the work of machine learning algorithms, or to do similar work without the need to write such programs in the first place. We are currently still identifying the best ways to apply VR further, but a promising avenue lies in the world of citizen science. VR has already been successfully used in citizen science [27] to detect disks around young stars. A citizen science based use of VR to recover NYMG members can provide a useful check on machine learning algorithms and statistical models such as BANYAN.

We also note that StarGateVR is still in very active development. We will continue to expand the scope of the tool and identify new applications. The methods outlines in this work can broadly apply to any other NYMG or nearby stellar association, and we will be investigating these groups as such in the future.

Additionally, we hope to further probe the solar neighborhood for very recently formed WDs. In addition to the NYMGs, there are also several older open clusters and large stellar streaming features [62] yet to be investigated. Our ultimate aim is to probe the ISM surrounding some of these WDs for remnants of their dispersed planetary nebulae.

Appendices

Appendix A

Table of New NYMG Candidates

A.1 Table Note

Star identifiers are given as catalogue IDs. Values of all measurements are obtained from . Errors in parallax, RA, DEC, PMRA, and PMDEC are small but may be obtained from the Gaia archive if necessary. Temperature and radii are derived from BT-Settl model fits [7] to each sources SED. Spectral types are estimated from [8], and corresponding masses may be found there.

Table A.1: Complete List of New Candidates With BT-Settl Modeled Temperature, Radii, and Estimated SpT

Group	Gaia DR3 ID	RA (deg)	DEC (deg)	ϖ (mas)	PMRA (mas yr^{-1})	PMDEC (mas yr^{-1})	RV (km s^{-1})	σ_{RV} (km s)	T_{eff} (K)	Radius ($R_\odot$)	SpT [63]
ABDMG	4899996487129314688	0.931	-65.78	29.451	137.941	-59.436	17.869	0.384	3500	0.466	M2.5V
ABDMG	2741802191422290176	1.605	4.837	19.729	88.275	-83.24	0.769	1.419	3200	0.371	M4V
ABDMG	4904674604163917696	3.982	-61.631	18.208	68.171	-41.96	24.465	2.025	3200	0.510	M4V
ABDMG	2792563894496829696	5.435	15.727	17.304	78.921	-74.694	-2.826	3.563	3200	0.355	M4V
ABDMG	524634348319029888	12.271	65.744	30.444	117.302	-61.535	-20.787	0.408	3900	0.440	K9V
ABDMG	4931809967022910976	13.965	-49.64	21.378	97.101	-56.467	20.405	2.426	3000	0.333	M5V
ABDMG	2787564449484699264	19.21	21.052	17.049	72.755	-76.768	-2.624	0.155	6700	1.526	F4V
ABDMG	2564275967417666944	20.098	5.252	16.989	72.319	-69.855	6.989	0.563	3800	0.525	M0.5V
ABDMG	292521529517332224	24.997	26.185	30.881	134.807	-151.966	-3.778	4.48	4100	0.426	K7V
ABDMG	518201792978856960	27.966	64.434	57.825	237.441	-193.607	-13.224	0.166	—	—	—
ABDMG	4940048264051817216	36.327	-46.914	15.512	68.883	-8.817	23.044	0.962	3600	0.472	M1.5V
ABDMG	2503139173839015936	38.813	2.797	39.903	125.543	-221.232	11.603	0.869	3000	0.333	M5V
ABDMG	65119748682966912	55.265	23.421	16.514	45.892	-98.082	6.654	0.469	4900	0.735	K3V
ABDMG	3243178943933047296	57.472	-8.071	15.45	47.335	-66.493	17.794	0.229	6300	1.188	F7V
ABDMG	63678907415301120	58.12	21.566	16.68	37.711	-106.111	8.653	0.821	3800	0.501	M0.5V
ABDMG	4779785132814476288	60.977	-54.354	12.44	27.577	-11.197	27.589	0.991	3800	0.522	M0.5V
ABDMG	4837065153135921024	64.483	-46.584	13.988	28.226	-11.707	28.888	1.225	4100	0.503	K7V

ABDMG	4884687028959710080	64.648	-30.492	20.607	57.235	-62.953	25.344	0.142	4900	0.717	K3V
ABDMG	3285622081332943232	67.854	6.256	15.899	25.962	-87.675	17.781	0.286	4400	0.755	K5V
ABDMG	3201018685961098240	68.646	-5.359	13.623	28.093	-63.481	19.449	4.226	3200	0.410	M4V
ABDMG	2979114871287464832	70.099	-17.345	14.978	30.967	-54.079	24.528	1.135	3600	0.531	M1.5V
ABDMG	4655541311014240128	72.548	-68.623	13.777	31.96	24.518	25.071	0.393	3800	0.755	M0.5V
ABDMG	2979189809876856064	73.154	-18.829	14.382	20.165	-52.37	25.818	0.245	4500	0.635	K5V
ABDMG	3226695615364589952	73.16	-0.996	16.959	12.605	-82.742	18.399	0.559	3700	0.576	M1V
ABDMG	3181460676205397120	73.331	-10.853	16.099	17.856	-71.942	25.097	3.215	3400	0.448	M3V
ABDMG	3186889171270161408	74.633	-7.933	13.57	13.542	-63.921	23.364	0.207	5600	0.890	G6V
ABDMG	4876845616972144512	76.05	-29.745	11.935	24.032	-25.883	28.069	0.221	5700	0.798	G3V
ABDMG	4823476460727785728	76.099	-37.506	23.53	51.603	-37.939	27.331	7.117	3200	0.494	M4V
ABDMG	4760652290461808640	77.296	-61.826	10.861	13.984	11.493	26.226	0.279	4700	0.739	K4V
ABDMG	4663740407899446656	77.743	-64.469	14.138	25.782	25.957	28.418	4.792	3500	0.502	M2.5V
ABDMG	2988451335618073856	78.032	-13.4	14.218	9.534	-60.287	24.306	0.857	4200	0.508	K6V
ABDMG	4800816419433104768	79.075	-42.226	20.089	36.478	-20.965	27.666	1.531	3300	0.474	M3.5V
ABDMG	2955348721294618368	80.241	-27.181	12.781	11.748	-34.366	27.738	3.352	3400	0.421	M3V
ABDMG	2905315960068496000	81.161	-30.924	13.426	11.94	-31.38	27.658	0.848	4200	0.667	K6V
ABDMG	4821532146212618752	81.466	-36.917	18.171	31.496	-24.629	27.331	27.209	3300	0.461	M3.5V
ABDMG	2908574259698392704	81.684	-27.27	12.157	12.775	-21.592	26.715	34.371	4000	0.506	K8V

ABDMG	2956669166040391040	81.853	-26.585	12.012	8.912	-33.702	29.483	0.164	7400	1.614	A9V
ABDMG	4798709067958473216	82.459	-47.076	19.55	28.183	-0.307	27.56	0.236	7200	1.476	F0V
ABDMG	4799260782277767296	82.925	-45.557	13.099	15.867	-8.807	30.745	0.652	4300	0.683	K6V
ABDMG	2905813763957931136	82.997	-29.771	14.026	7.674	-34.079	30.83	5.36	3100	0.314	M4.5V
ABDMG	3341555268631600256	84.209	13.632	17.615	4.897	-109.844	15.057	0.313	5100	0.713	K2V
ABDMG	4802945726778827520	84.329	-42.755	12.407	9.564	-10.092	30.671	4.252	3400	0.471	M3V
ABDMG	2900579779371768832	85.149	-33.801	12.527	1.852	-24.247	32.831	2.452	3600	0.485	M1.5V
ABDMG	2888253704268706688	85.466	-35.851	12.728	4.015	-20.317	35.819	4.719	3000	0.405	M5V
ABDMG	4808235953959731200	85.582	-39.561	10.838	9.117	-12.626	31.515	1.208	4400	0.578	K5V
ABDMG	4804760505079742336	85.627	-40.751	10.928	6.477	-10.642	29.544	10.305	5400	0.540	G9V
ABDMG	4804677796893551616	86.004	-41.252	11.348	6.04	-11.041	31.531	0.569	4800	0.688	K3V
ABDMG	2907676577173911424	86.033	-28.145	12.745	1.581	-29.529	28.052	0.447	4500	0.590	K5V
ABDMG	2915869966027648256	86.127	-23.605	13.834	1.973	-40.782	29.937	0.242	4800	0.712	K3V
ABDMG	4792199649884736896	86.791	-52.941	11.662	9.705	14.346	35.099	3.992	4200	0.617	K6V
ABDMG	2888847577986581888	86.831	-33.936	13.682	9.153	-18.714	28.293	3.248	3100	0.508	M4.5V
ABDMG	2904747237679167232	87.482	-27.817	12.292	12.64	-27.981	29.469	4.157	3400	0.396	M3V
ABDMG	4805020397844045568	87.494	-40.036	11.212	4.346	-12.631	31.715	0.396	5000	0.722	K2V
ABDMG	4794752612804490240	89.156	-48.792	17.457	18.138	-1.835	31.174	4.694	2900	0.476	M5.5V
ABDMG	2991678303464554368	89.192	-17.254	15.031	3.475	-47.683	23.462	4.108	3200	0.372	M4V

ABDMG	2909445897541101440	90.106	-28.938	12.946	4.451	-31.961	29.134	2.299	3600	0.478	M1.5V
ABDMG	5500304413985680768	90.231	-54.951	17.582	20.537	10.081	30.431	0.357	6600	1.358	F5V
ABDMG	2897361989873959168	90.659	-29.398	13.016	3.421	-31.399	26.926	2.704	3700	0.598	M1V
ABDMG	2883422621974755584	91.406	-37.414	15.426	0.792	-4.461	29.419	0.184	5400	0.791	G9V
ABDMG	2884574532203959808	92.564	-38.411	12.566	8.814	-13.175	33.368	5.518	3100	0.347	M4.5V
ABDMG	2993303106774038016	93.789	-15.025	15.313	-8.679	-56.154	28.925	1.553	4000	0.527	K8V
ABDMG	5574891984279264128	94.29	-37.254	15.965	-9.889	-23.145	28.907	0.463	7800	2.065	A7V
ABDMG	5481069007813444224	94.551	-61.933	12.957	3.94	24.521	31.348	2.884	4000	0.558	K8V
ABDMG	2898476654147271296	94.647	-28.302	16.105	-4.772	-34.305	26.974	18.665	3700	0.549	M1V
ABDMG	5495333556276171648	94.723	-57.323	11.072	4.868	15.903	30.706	1.311	3900	0.548	K9V
ABDMG	5550187572910255232	94.929	-50.329	14.138	12.514	3.041	28.853	1.078	4200	0.532	K6V
ABDMG	5554798134403541888	95.34	-46.736	12.176	12.069	-0.616	29.466	0.217	5500	0.846	G8V
ABDMG	5554798134403541760	95.341	-46.734	12.223	12.005	-0.844	30.085	1.986	4000	0.621	K8V
ABDMG	5478200588135044096	97.001	-62.154	11.943	1.488	24.917	33.201	5.227	3400	0.434	M3V
ABDMG	5280236955531554176	98.858	-67.921	12.008	-4.06	23.53	28.857	0.757	4400	0.556	K5V
ABDMG	937203855884408320	101.151	31.97	17.686	-14.679	-105.611	5.02	0.147	6500	1.154	F5V
ABDMG	3381634224106876672	102.752	25.759	29.068	10.801	-198.148	6.777	0.136	5800	1.280	G2V
ABDMG	2925888166229550464	102.827	-21.908	15.905	-19.417	-48.692	29.555	1.582	3900	0.502	K9V
ABDMG	3101905301926458752	103.164	-5.323	20.629	-25.752	-78.138	24.012	0.707	3600	0.526	M1.5V

ABDMG	3050922979271080576	103.522	-8.653	15.068	-22.848	-46.682	24.665	2.339	3400	0.472	M3V
ABDMG	5604179916030558464	107.127	-32.371	13.149	-15.499	-11.881	30.146	0.252	5000	0.734	K2V
ABDMG	5561375378603169024	108.223	-40.49	12.404	-10.617	-14.877	31.514	1.07	3700	0.591	M1V
ABDMG	5617595813322187264	108.393	-23.941	21.299	-19.206	-51.536	29.215	0.335	4800	0.792	K3V
ABDMG	5560192437231574784	108.736	-42.78	12.243	-14.274	5.798	30.698	0.287	4900	0.719	K3V
ABDMG	976478239429499264	110.456	47.997	20.359	-24.974	-118.816	-0.154	1.247	3500	0.390	M2.5V
ABDMG	5492410573334813184	114.261	-52.366	16.299	-31.968	6.151	31.44	0.207	6400	1.221	F6V
ABDMG	5592036497301929088	114.598	-32.501	13.572	-19.28	-11.202	28.94	1.802	6300	1.194	F7V
ABDMG	5214770723244296832	119.808	-74.185	14.063	-34.885	47.605	24.82	0.256	4700	0.699	K4V
ABDMG	5711271695744022272	120.256	-22.506	15.265	-29.673	-42.46	27.705	0.159	5000	0.772	K2V
ABDMG	5713693503244964480	121.555	-19.554	15.188	-47.291	-40.615	24.549	0.5	2300	21.172	L0V
ABDMG	5697953277039007616	121.87	-24.665	28.658	-83.813	-63.158	25.922	0.141	4900	0.767	K3V
ABDMG	3098004685640820352	123.324	7.791	17.879	-42.482	-102.939	12.713	0.209	3900	0.624	K9V
ABDMG	5513525835157867136	123.441	-49.92	11.905	-28.37	1.881	30.189	0.271	5200	0.733	K1V
ABDMG	677671008095729152	123.68	23.601	22.08	-52.296	-138.047	9.922	4.058	3400	0.341	M3V
ABDMG	5321369406350033664	126.481	-52.803	14.52	-37.937	2.399	30.483	0.679	4400	0.697	K5V
ABDMG	5302520551536567168	129.752	-59.619	14.25	-48.101	14.812	26.373	1.12	4700	0.733	K4V
ABDMG	5312552083330669824	141.953	-51.467	13.663	-43.731	-5.417	29.23	3.306	3300	0.470	M3.5V
ABDMG	5203782483211562496	145.201	-76.454	13.334	-47.065	12.418	26.731	0.443	3800	0.618	M0.5V

ABDMG	5657456442712755712	146.59	-27.276	18.874	-48.912	-65.916	23.577	0.152	6900	1.416	F2V
ABDMG	810593580116505728	153.824	47.429	24.545	-70.726	-120.475	-10.031	0.247	4000	0.496	K8V
ABDMG	5189160902706509696	155.052	-86.557	12.897	-47.916	28.298	23.63	0.316	6900	1.436	F2V
ABDMG	5191257877539468672	165.636	-84.491	14.565	-58.756	18.081	25.326	3.513	3000	0.384	M5V
ABDMG	861857244610039552	165.84	61.654	25.511	-116.934	-66.766	-15.749	4.685	6500	1.174	F5V
ABDMG	5336083762500221312	172.576	-59.987	32.935	-147.54	-66.112	21.392	1.182	3400	0.414	M3V
ABDMG	3951744987519137152	182.34	21.052	26.859	-104.733	-122.554	-8.94	1.101	3300	0.546	M3.5V
ABDMG	6186697667433011072	198.131	-27.04	34.693	-165.532	-159.302	6.473	0.338	3500	0.424	M2.5V
ABDMG	1552284674943267072	204.462	48.137	47.209	-241.458	-137.569	-20.161	0.221	3700	0.732	M1V
ABDMG	5864172256682581376	205.156	-64.07	14.978	-49.305	-47.285	18.279	0.181	6300	1.112	F7V
ABDMG	6002363001162403072	233.108	-41.796	18.262	-54.554	-104.306	0.276	5.442	3000	0.329	M5V
ABDMG	1192813951126183808	238.002	15.235	31.611	-56.556	-128.324	-23.164	0.132	5900	0.958	G0V
ABDMG	5778355236611770752	238.307	-79.627	14.43	-38.895	-60.839	16.131	6.668	3100	0.380	M4.5V
ABDMG	5764662880870489728	241.468	-89.309	12.778	-23.139	-40.599	23.159	0.167	6900	1.406	F2V
ABDMG	4325306090283827584	248.159	-15.988	23.581	-40.575	-132.527	-6.2	0.126	6300	1.314	F7V
ABDMG	1310150675243348736	256.425	31.119	25.944	-19.648	-52.549	-30.029	0.157	5100	0.800	K2V
ABDMG	5921599577133226240	263.647	-53.269	19.878	-25.915	-126.389	1.323	0.599	3700	0.551	M1V
ABDMG	4036773589046451584	268.602	-38.627	18.215	3.919	-122.247	-4.872	0.237	6700	1.415	F4V
ABDMG	4160922195665537792	276.205	-6.354	23.949	12.912	-108.699	-20.28	0.263	4400	0.722	K5V

ABDMG	4046709772499428608	278.84	-31.396	58.049	23.625	-383.091	-6.391	0.749	3000	0.429	M5V
ABDMG	2042228396309369088	283.284	31.797	28.92	46.452	-48.32	-29.596	0.153	4400	0.668	K5V
ABDMG	6366315952826621184	297.144	-76.097	16.818	25.961	-73.726	20.093	0.557	4200	0.570	K6V
ABDMG	6442084536047073664	297.278	-61.812	15.237	37.358	-95.89	8.052	0.193	4800	0.799	K3V
ABDMG	6690416968120938368	297.9	-40.423	35.204	55.528	-197.285	2.432	1.177	3200	0.424	M4V
ABDMG	4304136333937439488	298.357	12.179	17.317	25.864	-67.144	-21.705	4.457	3200	0.338	M4V
ABDMG	6422432518048366976	298.489	-71.406	12.966	19.277	-70.136	13.869	2.945	5600	0.486	G6V
ABDMG	6427284422343978368	299.871	-67.201	20.63	36.645	-105.766	11.994	0.173	4200	0.641	K6V
ABDMG	1829403940648464384	304.074	22.102	19.46	48.054	-55.625	-23.712	0.176	5000	0.794	K2V
ABDMG	6795871055324926592	312.081	-28.025	17.061	46.886	-103.424	-3.173	0.791	3900	0.717	K9V
ABDMG	6795871059622986240	312.082	-28.025	16.768	40.417	-92.297	-8.473	3.176	3200	0.791	M4V
ABDMG	6788428809012385536	315.357	-29.978	14.143	35.882	-82.576	-0.056	1.936	3100	0.583	M4.5V
ABDMG	6788428809012385408	315.358	-29.978	14.151	32.757	-83.849	-3.646	2.63	3000	0.528	M5V
ABDMG	6917117913373156480	315.966	-1.548	16.742	40.259	-84.03	-16.906	0.759	3900	0.508	K9V
ABDMG	1760316677257596288	316.453	15.327	21.339	84.973	-80.218	-21.925	0.134	6400	1.695	F6V
ABDMG	6787949937336590080	319.522	-29.514	21.983	55.952	-135.944	-4.074	0.15	5700	0.898	G3V
ABDMG	1797312357315620352	322.196	23.336	20.643	62.304	-81.559	-20.951	0.284	4200	0.668	K6V
ABDMG	6785220605879225344	323.361	-30.395	20.281	62.287	-115.616	-0.234	2.796	3000	0.326	M5V
ABDMG	6403254252120730368	323.719	-63.02	27.795	111.928	-147.461	12.881	0.274	3300	0.491	M3.5V

ABDMG	6831554747427433728	324.338	-18.442	17.939	55.606	-104.84	-0.721	0.136	6800	1.389	F2V
ABDMG	2674359621346653824	324.588	-2.181	15.166	47.585	-68.895	-15.545	0.35	4700	0.514	K4V
ABDMG	6810749341730012544	325.809	-27.47	21.683	86.971	-119.821	2.179	1.115	2400	0.709	M8.5V
ABDMG	6562535382034641792	326.817	-48.045	15.923	50.012	-85.065	8.357	2.431	3200	0.381	M4V
ABDMG	6586580842340695040	329.333	-37.764	22.269	101.032	-118.842	5.606	0.122	6100	1.188	F9V
ABDMG	1975678603914495616	331.524	47.568	26.999	101.231	-65.968	-23.518	2.102	3100	0.497	M4.5V
ABDMG	6511622010777371776	333.619	-50.031	15.774	56.967	-77.82	8.411	0.611	3900	0.554	K9V
ABDMG	1934349508007052928	343.751	42.495	23.076	103.222	-50.557	-21.541	0.137	5400	0.821	G9V
ABDMG	2663445770145454848	345.637	5.718	21.974	99.05	-87.771	-11.581	0.187	4200	0.595	K6V
ABDMG	6377390543178333056	354.67	-77.158	23.37	94.265	-50.247	22.189	5.411	3000	0.270	M5V
ABDMG	2878196299610044032	356.646	34.457	17.493	83.567	-55.097	-13	0.902	3400	0.476	M3V
ABDMG	6534422175381498496	358.035	-39.777	16.29	74.562	-63.369	13.922	1.354	3300	0.378	M3.5V
ABDMG	2847644410526748416	358.862	22.193	39.256	202.046	-147.05	-11.655	0.136	4700	0.741	K4V
ARG	512167948043650816	26.943	63.851	99.59	581.684	-246.462	2.615	0.12	—	—	—
ARG	5279746843928722432	92.644	-68.998	22.081	10.273	124.467	14.693	3.85	3000	0.237	M5V
ARG	5505536989823914240	108.72	-49.198	13.758	-20.672	59.996	19.669	0.614	3600	0.598	M1.5V
ARG	5487374844438857728	110.095	-56.294	13.741	-27.01	61.408	13.928	0.39	9600	1.505	A0V
ARG	5288873928599788288	112.807	-62.514	14.586	-36.576	62.097	11.329	1.764	4700	1.200	K4V
ARG	5277389495292275712	121.226	-63.771	13.852	-40.347	60.305	10.442	3.27	3900	0.719	K9V

ARG	5595942787244790528	121.44	-31.52	14.663	-29.939	33.464	21.744	1.251	3900	0.715	K9V
ARG	5596414164188103552	122.05	-30.375	17.028	-46.627	40.464	22.873	0.802	3400	0.613	M3V
ARG	5315691670041169920	124.127	-57.659	11.956	-31.844	53.128	16.929	5.8	3600	0.569	M1.5V
ARG	5539990564641567488	125.153	-40.202	8.107	-25.67	24.936	15.327	10.268	4100	0.669	K7V
ARG	5515292303669259776	126.319	-49.232	7.766	-26.036	27.369	19.475	7.01	3400	0.503	M3V
ARG	5302148607365884928	126.783	-61.075	8.942	-30.777	36.909	12.219	4.538	3600	0.743	M1.5V
ARG	5316163051297868288	127.952	-55.842	10.245	-36.424	38.166	15.804	4.745	3500	0.583	M2.5V
ARG	5273059412344126208	128.02	-65.668	9.067	-26.224	41.695	14.524	0.238	6300	1.277	F7V
ARG	5304502489970688896	132.02	-57.289	7.708	-28.907	27.828	8.537	6.064	3500	0.672	M2.5V
ARG	5524672443520376960	133.296	-41.454	7.897	-30.284	18.593	21.238	6.84	3500	0.568	M2.5V
ARG	5296630635245171712	134.024	-64.659	10.436	-42.843	39.498	8.794	5.447	3200	0.435	M4V
ARG	5296630639541459072	134.028	-64.66	10.522	-40.583	39.868	10.943	0.267	6100	1.110	F9V
ARG	5304948960420921856	135.779	-55.353	7.278	-29.497	23.94	8.803	6.641	3600	0.649	M1.5V
ARG	5624801875084229888	136.936	-34.122	10.82	-39.349	25.171	18.044	0.152	6600	1.567	F5V
ARG	5324054899083453184	136.958	-51.093	9.694	-46.7	24.397	16.897	2.478	3600	0.533	M1.5V
ARG	5300158800568108928	136.994	-59.331	7.381	-30.759	23.737	9.39	4.995	3400	0.624	M3V
ARG	5327462045096640512	138.796	-46.217	8.462	-31.712	21.824	10.691	5.286	1700	37.099	L5V
ARG	5430803218846586752	140.478	-38.221	9.501	-39.658	19.311	13.901	4.627	3400	0.540	M3V
ARG	5250419123598416384	141.684	-63.303	13.726	-60.245	43.917	10.762	1.378	4200	0.677	K6V

ARG	5423284895776354944	141.779	-44.887	12.838	-62.254	27.113	17.971	1.703	3600	0.536	M1.5V
ARG	5429985353994214656	141.916	-38.565	8.46	-37.416	15.413	16.113	0.747	5400	0.807	G9V
ARG	5430194020684537600	142.173	-37.547	9.201	-39.989	17.81	14.338	5.247	3400	0.434	M3V
ARG	5305321385626888704	143.544	-59.733	13.239	-52.739	39.481	12.233	7.928	3000	0.318	M5V
ARG	5432954688222466560	145.284	-37.728	10.802	-44.48	24.157	13.437	6.472	3300	0.422	M3.5V
ARG	5411459235907313920	146.101	-46.356	9.14	-34.892	18.616	8.982	7.688	3600	0.538	M1.5V
ARG	5409456509842909056	146.157	-49.288	11.734	-53.942	23.97	14.467	3.323	3200	0.311	M4V
ARG	5309383428248088576	147.138	-52.765	13.205	-61.767	40.659	8.295	5.063	3200	0.312	M4V
ARG	5459488824377831552	150.501	-34.173	13.182	-52.398	20.184	10.436	0.156	7600	1.607	A8V
ARG	5414791305890832000	150.879	-45.079	9.793	-45.389	13.144	16.452	0.399	4600	0.704	K4V
ARG	5355225430953923584	153.984	-55.496	8.082	-39.798	17.768	4.832	4.722	3900	0.815	K9V
ARG	5416456069571762816	155.46	-41.983	23.339	-125.74	12.365	12.118	1.79	3100	0.357	M4.5V
ARG	5232109922839642368	158.862	-70.311	15.07	-84.723	35.567	4.2	3.674	3400	0.457	M3V
ARG	5228879798191489152	161.975	-73.787	11.038	-59.161	18.766	1.242	6.52	3400	0.468	M3V
ARG	5338237327817885696	163.714	-60.265	9.03	-44.78	18.404	3.313	7.331	3900	0.477	K9V
ARG	5226381978352399104	164.851	-73.031	20.464	-111.254	28.817	1.516	3.129	3300	0.630	M3.5V
ARG	5226381982652636928	164.854	-73.03	20.487	-110.612	27.591	5.843	3.346	3000	0.292	M5V
ARG	5390527180204478720	166.646	-39.481	21.117	-115.502	-4.096	7.825	2.051	3200	0.348	M4V
ARG	5228613578945446784	167.575	-70.384	12.081	-70.153	25.254	5.516	0.396	5000	0.944	K2V

ARG	5334792454825802624	177.703	-61.35	10.615	-65.905	5.791	5.977	0.378	4700	0.812	K4V
ARG	5867265350307448448	210.729	-60.346	12.545	-64.072	-25.593	-3.996	0.133	6400	1.376	F6V
ARG	5798278799637597952	218.275	-70.202	13.84	-61.606	-39.067	-3.285	0.19	5400	0.816	G9V
ARG	5793564093770947584	225.939	-73.532	14.21	-54.9	-56.058	-6.315	3.38	2900	0.380	M5.5V
ARG	6000034407338331520	229.556	-45.477	15.658	-64.96	-48.806	-14.52	4.199	3000	0.324	M5V
ARG	4408913744737288320	244.796	1.678	44.896	-150.39	-12.994	-24.133	2.647	3100	0.295	M4.5V
ARG	5808315755939485696	252.081	-69.539	15.354	-26.601	-77.881	-8.899	0.904	3900	0.761	K9V
ARG	4128708566525738112	254.564	-20.204	22.473	-53.909	-47.867	-20.914	0.5	3400	0.441	M3V
ARG	4111704752334176384	261.67	-22.631	22.966	-7.93	-54.37	-20.927	0.845	3400	0.516	M3V
ARG	4369747594365857408	262.78	-2.655	36.563	-44.736	-22.285	-28.448	1.273	3100	0.301	M4.5V
ARG	4372709335095064448	267.984	1.706	36.588	-33.09	-16.471	-26.146	4.439	1500	0.408	L7V
ARG	4070316832559678208	269.915	-21.992	15.645	-13.632	-35.854	-23.389	2.187	3400	0.461	M3V
ARG	6702762903160966912	273.234	-50.559	14.958	-1.372	-79.856	-13.102	1.106	7000	2.137	F1V
ARG	4048539222453527552	277.514	-28.602	21.206	9.507	-75.94	-25.118	4.562	3000	0.302	M5V
ARG	6716791228414290944	284.254	-40.198	42.258	34.06	-192.547	-19.787	1.215	3000	0.325	M5V
ARG	2046207670631964928	290.892	33.223	64.07	81.966	160.158	-21.623	0.118	5400	0.917	G9V
ARG	2064015945060729472	308.399	38.895	27.091	103.943	56.47	-19.483	0.307	2900	0.528	M5.5V
ARG	2161733975835084544	314.907	42.045	36.026	111.58	106.876	-11.024	0.151	4400	0.693	K5V
βPMG	2797571482766220160	4.914	19.851	17.376	72.366	-44.471	-6.162	1.769	3100	0.474	M4.5V

βPMG	4906761820830908032	9.004	-59.717	17.558	78.007	-17.228	14.721	0.192	7000	1.481	F1V
βPMG	565706429072383232	16.733	80.459	46.931	206.667	-25.257	-12.327	2.262	3200	0.353	M4V
βPMG	2558125161933375104	22.27	0.516	18.436	51.952	-28.771	9.53	2.308	3100	0.385	M4.5V
βPMG	303793555221824640	24.582	31.381	13.302	45.515	-50.229	1.419	0.304	6200	0.975	F8V
βPMG	2504554451462345600	27.902	-2.638	15.285	70.577	-25.185	9.562	0.277	7000	1.532	F1V
βPMG	123185851098826880	46.717	30.527	13.494	38.258	-51.331	5.248	0.634	6900	0.233	F2V
βPMG	16983468919490176	48.697	11.457	17.634	60.455	-45.099	8.943	2.042	3600	0.821	M1.5V
βPMG	9124679495764864	50.914	5.687	26.638	83.321	-69.497	12.158	1.458	3700	0.423	M1V
βPMG	118821167893453696	51.039	27.794	12.929	35.2	-49.243	10.635	3.493	3400	0.496	M3V
βPMG	61801491310173056	51.879	22.21	25.896	66.668	-80.368	10.697	0.945	4100	0.353	K7V
βPMG	3311206862213846144	65.607	14.925	14.413	39.161	-46.598	12.839	2.839	3200	0.554	M4V
βPMG	3307516248356072960	68.776	13.134	13.062	24.039	-46.226	17.971	2.219	3100	0.622	M4.5V
βPMG	3234516097975452672	79.211	2.454	17.313	28.189	-46.224	13.11	4.577	3100	0.512	M4.5V
βPMG	3320316831446869888	86.258	4.008	16.909	3.071	-39.606	10.433	0.522	7200	2.132	F0V
βPMG	4792149175429007360	88.121	-53.05	20.374	24.622	36.592	21.731	1.585	3300	0.559	M3.5V
βPMG	6016786291603048320	236.448	-30.349	25.727	-69.393	-99.841	-5.749	0.36	4400	1.138	K5V
βPMG	5826466047245658240	236.531	-62.968	17.013	-42.776	-61.791	2.526	2.381	2900	0.488	M5.5V
βPMG	5972194910385133184	258.067	-39.507	15.612	-14.182	-71.513	-0.86	0.329	8800	1.857	A2V
βPMG	4117562572327410432	263.518	-22.504	15.282	-3.358	-50.165	-7.014	3.761	1500	0.154	L7V

βPMG	4161560427799517184	264.444	-13.247	30.108	-17.393	-126.177	-17.113	2.607	4100	0.838	K7V
βPMG	4060162327281216896	265.099	-28.948	10.968	-2.705	-39.006	-11.991	4.888	3900	0.963	K9V
βPMG	4060162331630245888	265.101	-28.947	10.96	-3.035	-40.05	-7.286	1.958	3200	0.772	M4V
βPMG	5961097230314565760	265.675	-39.877	8.471	-2.941	-33.065	-6.378	5.117	1700	1.069	L5V
βPMG	5955638464288020352	266.805	-43.363	8.454	-9.771	-37.112	-5.693	8.713	3500	0.902	M2.5V
βPMG	4057219042072522496	267.615	-29.474	10.092	0.419	-44.838	-7.731	0.799	4000	0.857	K8V
βPMG	5956507726972104192	267.642	-42.849	8.419	-2.191	-33.537	-3.071	4.536	4200	0.984	K6V
βPMG	4070354804376104192	269.145	-21.988	10.083	-9.872	-35.251	-8.955	5.001	3100	2.117	M4.5V
βPMG	4066318531598567424	272.626	-23.567	9.883	-4.931	-39.349	-7.231	0.357	6100	1.897	F9V
βPMG	6721371896953755776	273.339	-43.672	8.409	0.889	-33.95	-2.643	2.451	3900	0.813	K9V
βPMG	6721371892640117888	273.343	-43.671	8.409	1.106	-32.896	-9.049	4.633	3300	0.614	M3.5V
βPMG	6728181206848748672	274.647	-37.171	25.279	-12.192	-108.089	-3.32	8.234	3100	0.547	M4.5V
βPMG	4053144110202691840	276.102	-25.376	10.182	-2.9	-41.946	-10.083	7.195	3400	1.268	M3V
βPMG	4048015232057762432	276.163	-29.759	10.045	-3.332	-42.679	-9.98	7.807	4000	0.974	K8V
βPMG	6765662080732001664	290.796	-27.57	12.721	19.018	-47.69	-14.377	3.823	3400	0.587	M3V
βPMG	6771833639498793600	294.012	-22.506	10.05	23.547	-36.011	-14.49	0.413	5800	0.971	G2V
βPMG	6468991303565458816	307	-56.163	14.15	29.031	-53.208	4.177	10.699	3300	0.703	M3.5V
βPMG	6695180705328058752	308.103	-36.687	13.285	33.494	-61.181	-6.973	3.915	3200	0.438	M4V
βPMG	1857250172128937856	308.994	27.867	25.504	37.196	-22.292	-19.78	25.449	2900	0.439	M5.5V

βPMG	6455829427826823168	311.201	-58.058	16.066	39.319	-56.755	3.021	2.455	3000	0.490	M5V
βPMG	6677117412912325248	312.298	-42.393	12.46	44.901	-39.428	-2.168	4.707	3400	0.440	M3V
βPMG	6481430353489019776	314.946	-48.165	11.945	25.74	-44.215	4.991	2.06	3000	0.766	M5V
βPMG	2666647337551843584	325.658	-7.746	14.037	33.47	-29.564	-11.981	0.396	4800	1.026	K3V
βPMG	2697437477060222720	328.664	6.044	15.511	44.754	-32.768	-11.499	0.464	3400	0.683	M3V
βPMG	2718224195355526144	342.384	10.478	15.286	65.828	-36.147	-9.438	0.477	7600	1.779	A8V
βPMG	2419885149815948416	355.681	-14.545	20.895	98.578	-66.231	-0.116	2.745	10200	2.088	B9.5V
CAR	5260885172922381824	103.453	-75.704	10.965	4.632	40.004	17.246	9.17	3400	0.620	M3V
CAR	5264023999444318464	108.759	-72.047	10.868	0.324	37.305	19.489	0.718	5500	1.084	G8V
CAR	5292317736459053312	113.806	-61.455	9.095	-3.824	24.815	23.198	8.493	3800	0.734	M0.5V
CAR	5293469573671058944	114.002	-59.608	9.545	-4.992	24.477	23.2	2.158	5200	0.759	K1V
CAR	5295406539500691072	115.026	-57.923	7.755	-3.79	19.652	24.186	0.701	4100	0.961	K7V
CAR	5289238756006614272	115.507	-62.043	10	-6.058	26.981	21.402	1.777	4100	0.709	K7V
CAR	5287488956268709888	115.771	-64.475	9.823	-5.967	28.049	22.664	4.13	3400	0.655	M3V
CAR	5275773488076705024	116.7	-65.12	9.589	-6.262	28.035	20.053	11.937	3400	0.553	M3V
CAR	5287921923332236800	117.414	-63.7	9.566	-7.034	26.803	22.953	7.653	3300	0.453	M3.5V
CAR	5295599194554272768	117.598	-56.326	8.12	-6.437	18.881	21.95	2.113	6900	1.472	F2V
CAR	5290900569051575424	118.223	-60.786	8.917	-6.892	23.158	21.752	0.547	6000	0.922	F9.5V
CAR	5290604044511975040	118.406	-61.882	9.081	-8.515	23.089	21.604	2.722	3500	0.611	M2.5V

CAR	5488393267085781888	119.303	-54.455	7.933	-6.743	17.963	24.287	0.813	4800	0.836	K3V
CAR	5291550174265854208	120.519	-58.726	8.748	-6.924	22.859	22.348	0.407	5400	0.869	G9V
CAR	5269346361575307264	121.314	-71.103	10.75	-13.531	32.517	19.006	0.974	4400	0.910	K5V
CAR	5291385213162538624	122.656	-59.012	8.709	-9.598	21.332	23.995	2.522	3500	0.577	M2.5V
CAR	5291438745634787328	123.127	-58.43	8.951	-10.885	21.114	22.364	4.112	3400	0.561	M3V
CAR	5277526934245765376	123.193	-63.077	8.322	-9.157	22.321	21.79	6.387	3500	0.592	M2.5V
CAR	5319254603112221952	123.262	-55.149	7.808	-9.066	16.721	19.976	5.873	3500	0.535	M2.5V
CAR	5315521619400416128	125.689	-57.887	7.684	-9.783	18.032	20.332	1.475	5300	0.861	K0V
CAR	5315521623693736064	125.692	-57.889	7.742	-10.004	17.539	21.907	0.169	7800	1.623	A7V
CAR	5319468114529032448	126.547	-54.797	7.791	-10.989	15.922	22.786	0.443	5000	0.929	K2V
CAR	5276668658041488640	127.483	-63.585	8.381	-12.283	20.99	22.207	0.77	5100	1.015	K2V
CAR	5321126826600019584	127.579	-53.281	7.292	-11.294	14.028	23.056	2.46	4000	0.699	K8V
CAR	5321530317305022464	127.59	-51.701	8.247	-11.409	15.614	23.349	0.437	5300	0.814	K0V
CAR	5321553024789777792	127.663	-51.684	7.6	-11.682	14.046	23.514	0.631	6000	1.013	F9.5V
CAR	5219822639873434112	129.114	-74.354	10.894	-16.725	35.234	17.457	0.671	4800	0.800	K3V
CAR	5301705916499514752	131.301	-60.12	7.534	-13.126	17.274	20.201	2.621	6000	0.640	F9.5V
CAR	5220464995182613120	131.521	-72.486	10.665	-18.373	32.473	16.346	5.484	3700	0.731	M1V
CAR	5301812603489357440	132.118	-59.687	7.32	-12.603	16.282	22.485	2.043	4700	0.949	K4V
CAR	5327902021551151872	132.672	-50.286	8.006	-15.651	12.283	23.103	1.963	3900	0.697	K9V

CAR	5297822922465031424	133.015	-62.815	7.837	-14.105	18.863	19.779	3.252	3600	0.670	M1.5V
CAR	5223228170984191360	134.343	-69.642	9.196	-16.693	25.74	19.086	1.273	7600	1.556	A8V
CAR	5296337069936389248	134.405	-65.455	7.846	-17.99	19.777	20.923	4.56	3500	0.929	M2.5V
CAR	5298425111243573376	134.7	-61.254	7.207	-12.626	13.325	21.523	4.294	3800	1.653	M0.5V
CAR	5298349829055280384	134.779	-61.771	7.702	-14.869	18.04	21.002	2.963	4200	0.756	K6V
CAR	5298170093266064128	136.2	-61.813	8.143	-16.767	18.104	17.946	3.303	3500	0.655	M2.5V
CAR	5304828971900544896	136.21	-56.294	12.413	-27.301	15.239	21.51	3.185	3900	0.717	K9V
CAR	5309768154242210304	138.787	-57.009	7.232	-15.405	11.773	19.105	1.726	5800	1.152	G2V
CAR	5310200502835788800	138.812	-55.198	7.347	-16.98	11.684	23.1	3.529	5800	0.969	G2V
CAR	5311475867608653696	139.125	-53.672	7.297	-17.296	10.949	22.129	2.618	3800	0.748	M0.5V
CAR	5310658758672519168	139.266	-54.714	7.484	-17.54	12.139	21.686	0.957	5200	0.875	K1V
CAR	5310641510088428672	139.895	-54.478	7.213	-17.323	11.147	22.872	7.984	3400	0.595	M3V
CAR	5248443958340243584	140.752	-65.526	8.088	-18.791	17.92	21.081	0.744	6500	1.565	F5V
CAR	5310518605301690368	141.228	-54.651	7.347	-18.126	10.868	21.008	0.807	5200	1.020	K1V
CAR	5248642003570725760	141.688	-64.631	8.479	-20.502	17.699	19.916	1.716	4400	0.757	K5V
CAR	5307225121291062912	142.007	-56.267	7.3	-18.049	11.529	22.661	7.437	3600	0.739	M1.5V
CAR	5306646262777290112	142.121	-56.731	7.522	-18.545	12.002	20.351	3.533	3700	0.698	M1V
CAR	5312422272235415040	142.268	-52.532	7.566	-19.509	9.582	20.145	4.508	3500	0.721	M2.5V
CAR	5313722960120541312	142.417	-50.659	7.929	-20.512	9.161	21.367	1.315	5000	1.021	K2V

CAR	5307491718499561600	142.515	-54.392	7.294	-18.919	10.173	19.233	3.57	3900	0.674	K9V
CAR	5308691040849641472	144.266	-55.333	7.671	-20.196	10.442	20.344	0.718	4800	0.911	K3V
CAR	5309576014589472640	144.744	-52.516	7.296	-19.886	8.72	20.507	2.681	4600	0.887	K4V
CAR	5305417489798168704	145.21	-59.227	7.151	-19.103	11.617	19.758	1.016	5500	0.883	G8V
CAR	5257782248057534208	146.508	-58.744	7.411	-20.488	12.609	21.484	0.318	7000	1.496	F1V
CAR	5256842543566317312	146.928	-61.501	7.734	-20.329	14.273	16.671	4.672	3600	0.471	M1.5V
CAR	5257527539324149632	147.699	-59.082	7.25	-20.577	10.484	21.543	6.272	3600	0.748	M1.5V
CAR	5257392295070412032	148.556	-60.275	11.835	-30.956	15.052	18.388	1.77	4200	0.768	K6V
CAR	5259312012313189376	149.473	-57.417	9.737	-29.847	8.958	19.335	0.51	5100	0.990	K2V
CAR	5246295959308854400	152.082	-65.259	8.205	-24.434	14.139	18.931	0.843	5900	1.074	G0V
CAR	5246284685000163968	152.695	-65.38	9.227	-24.531	14.381	18.905	3.154	6600	0.588	F5V
CAR	5245106150284051712	154.266	-67.071	7.237	-23.298	11.724	17.432	4.317	3900	0.737	K9V
CAR	5254610741146248448	156.66	-61.487	9.422	-27.486	9.432	18.904	7.357	3400	0.551	M3V
CAR	5241865163655827968	164.017	-61.868	11.591	-42.042	5.168	17.006	0.571	4400	0.943	K5V
COL	4700754191218621184	32.625	-63.747	10.022	39.231	3.766	15.472	5.922	3500	0.483	M2.5V
COL	4721257853989553152	40.525	-63.581	9.818	40.264	3.16	14.587	4.221	3400	0.694	M3V
COL	4721962812741729792	44.762	-61.333	13.31	55.879	7.532	17.166	3.151	3100	0.456	M4.5V
COL	4734504112949828992	46.199	-55.033	10.377	40.468	2.19	16.146	1.398	4300	0.790	K6V
COL	4734702957052109184	46.203	-54.739	11.414	41.693	0.886	16.194	4.92	3000	0.496	M5V

COL	5154992101403310080	49.387	-15.086	13.692	53.584	-23.998	15.872	0.385	4600	0.869	K4V
COL	5100211575953053824	50.415	-20.327	10.423	39.413	-14.096	16.533	0.992	4000	0.962	K8V
COL	11536458251396352	54.031	8.812	9.718	38.796	-26.478	14.768	4.314	4500	0.453	K5V
COL	5085456649601834240	54.757	-24.568	17.167	67.019	-19.334	16.548	4.622	2800	0.572	M6V
COL	5087979238513395072	55.317	-22.879	13.964	49.708	-16.38	16.843	3.075	3800	0.684	M0.5V
COL	4667876873699016576	57.368	-67.465	11.804	42.03	19.349	18.009	2.256	3500	0.585	M2.5V
COL	4841875168613813248	59.15	-42.555	10.558	34.997	1.973	20.736	4.878	3300	0.507	M3.5V
COL	4838127105273791616	61.706	-45.16	13.264	41.791	9.773	22.623	3.574	3300	0.888	M3.5V
COL	4682035388008718976	61.787	-57.729	14.368	47.454	18.781	19.96	1.483	3200	0.629	M4V
COL	5089529721705932288	62.105	-22.877	11.415	38.516	-11.03	21.269	36.745	3600	0.728	M1.5V
COL	3202619471812049536	64.545	-4.915	10.178	32.681	-20.776	20.612	0.422	6100	1.083	F9V
COL	2978678635751304192	70.212	-18.707	13.518	36.886	-14.041	21.58	0.983	3600	0.749	M1.5V
COL	3184299134191645056	70.978	-10.575	15.065	45.934	-24.638	18.775	3.435	3000	0.405	M5V
COL	3179832780521841152	72.548	-13.649	9.931	27.398	-12.218	23.842	4.848	3700	0.715	M1V
COL	3226601229163240960	72.669	-1.263	8.266	22.839	-17.309	18.929	2.416	3800	0.732	M0.5V
COL	4761798943650247552	72.81	-60.308	9.967	25.951	19.742	20.194	1.266	4300	0.732	K6V
COL	2987443461411633024	74.703	-14.318	11.043	28.011	-13.529	19.101	5.324	3100	0.551	M4.5V
COL	2987443461411599488	74.704	-14.315	11.103	27.505	-13.239	21.409	2.683	3900	0.714	K9V
COL	4664791781510322304	74.773	-63.425	11.618	27.514	27.246	18.191	0.767	4600	1.072	K4V

COL	2973162115335027200	75.119	-22.028	10.974	27.391	-6.475	23.437	0.821	4400	0.823	K5V
COL	3238551507511143424	76.149	4.046	8.221	21.531	-22.05	21.459	0.35	5900	0.966	G0V
COL	4764436225368768384	77.889	-55.86	12.207	28.265	23.158	20.744	6.882	3400	0.441	M3V
COL	3207847890121506560	77.95	-7.549	13.03	31.607	-24.548	20.061	4.252	3100	0.416	M4.5V
COL	3014411427921646080	78.902	-9.514	12.198	31.738	-18.416	20.658	0.329	5800	0.943	G2V
COL	2969283038313232384	79.507	-19.94	9.691	19.406	-6.822	26.063	3.374	3600	0.703	M1.5V
COL	4769544865628780800	80.523	-55.826	12.322	25.468	22.994	20.174	2.101	3300	0.689	M3.5V
COL	3015014578769945344	80.935	-7.894	8.969	15.975	-13.993	23.313	3.454	3900	0.968	K9V
COL	2982142101676081024	81.119	-16.976	14.189	33.388	-16.837	22.393	0.699	9800	1.867	A0V
COL	2984119023582957824	81.903	-15.036	12.147	20.561	-14.755	22.573	4.097	2900	0.409	M5.5V
COL	2970047886086738432	82.008	-17.422	12.836	30.026	-11.913	21.735	4.207	3400	0.533	M3V
COL	2905450822041518976	83.262	-30.575	8.834	17.576	2.957	25.177	1.531	4300	0.716	K6V
COL	4759420699999296384	83.649	-60.183	13.82	25.17	33.032	18.406	2.762	3000	0.612	M5V
COL	2907627855064856064	84.388	-27.585	8.614	14.966	0.384	23.191	1.653	3500	2.466	M2.5V
COL	4759320919319218432	85.249	-61.1	12.885	21.743	32.865	20.048	4.706	3300	0.804	M3.5V
COL	4759320919319218560	85.25	-61.101	12.946	23.677	30.948	21.122	1.238	3400	0.900	M3V
COL	2966979973769153280	85.893	-19.491	9.332	15.183	-5.146	24.715	2.494	3400	0.536	M3V
COL	2966979527092556032	85.903	-19.507	9.417	15.63	-5.951	26.936	2.821	3200	0.653	M4V
COL	4767595019195868288	86.825	-54.841	11.414	19.621	25.931	22.379	0.222	6100	1.307	F9V

COL	2965857887793178752	87.547	-20.726	9.948	9.126	-7.805	23.445	4.831	3700	0.617	M1V
COL	4792137974154287104	87.679	-53.144	25.404	38.884	39.229	22.726	3.979	3100	0.450	M4.5V
COL	4803396075572557696	87.841	-43.702	8.82	12.143	13.675	24.782	0.814	4400	0.894	K5V
COL	3022113124619680768	88.152	-5.931	13.258	12.005	-26.048	23.767	2.543	3700	0.753	M1V
COL	2898508814862920576	95.552	-28.314	12.708	13.639	-0.563	26.962	9.822	3600	0.683	M1.5V
COL	5496804462316135168	100.317	-56.275	16.345	4.889	35.651	21.039	5.263	3100	0.604	M4.5V
THA	4900997562402606208	7.606	-62.601	22.544	96.465	-52.382	5.993	2.944	3300	0.548	M3.5V
THA	3261733202649972992	49.17	-3.53	20.367	82.097	-49.047	10.208	0.479	6100	1.293	F9V
THA	5047297067767149056	49.21	-35.161	21.412	83.526	-17.412	12.573	5.286	3300	0.781	M3.5V
THA	4790875077673493760	68.442	-45.19	20.024	61.762	9.005	18.017	1.043	3400	0.608	M3V
THA	4879882953420860672	73.407	-28.592	16.294	37.858	-3.093	18.198	3.57	3200	0.848	M4V
THA	5766835408470793984	227.069	-84.566	15.835	-59.956	-26.606	11.318	0.275	4400	0.772	K5V
THA	6645159798213038976	292.615	-53.441	20.79	-0.534	-97.945	-2.567	3.471	2800	0.463	M6V
THOR	3294687387202450432	72.217	10.51	10.828	17.196	-36.994	16.674	2.264	4100	0.857	K7V
THOR	3393804134197211520	78.263	15.801	9.882	11.76	-36.415	17.876	3.407	3100	0.576	M4.5V
THOR	3242213435283849856	79.797	8.368	9.274	8.844	-30.834	21.373	4.671	3300	0.617	M3.5V

Bibliography

[1] Jonathan Gagné, Eric E. Mamajek, Lison Malo, Adric Riedel, David Rodriguez, David Lafrenière, Jacqueline K. Faherty, Olivier Roy-Loubier, Laurent Pueyo, Annie C. Robin, and René Doyon. BANYAN. XI. The BANYAN Σ Multivariate Bayesian Algorithm to Identify Members of Young Associations with 150 pc. , 856(1):23, March 2018. (document), 1.1, 2.4

[2] B. Zuckerman. The Nearby, Young, Argus Association: Membership, Age, and Dusty Debris Disks. , 870(1):27, January 2019. (document), 1.1, 2.4, 3.1, 3.4

[3] Jonathan Gagné, Jacqueline K. Faherty, and Eric E. Mamajek. Volans-Carina: A New 90 Myr Old Stellar Association at 85 pc. , 865(2):136, October 2018. (document), 1.1

[4] Jinhee Lee and Inseok Song. Evaluation of nearby young moving groups based on unsupervised machine learning. , 489(2):2189–2194, October 2019. (document), 2.1, 2.1.1, 2.2.2.1, 3.4, 4.2

[5] Jinhee Lee, Inseok Song, and Simon Murphy. 2MASS J15460752-6258042: a mid-M dwarf hosting a prolonged accretion disc. , 494(1):62–68, May 2020. (document), 3.2, 3.1

[6] Alessandro Bressan, Paola Marigo, Léo. Girardi, Bernardo Salasnich, Claudia Dal Cero, Stefano Rubele, and Ambra Nanni. PARSEC: stellar tracks and isochrones with the PAdova and TRieste Stellar Evolution Code. , 427(1):127–145, November 2012. (document), 3.4

[7] F. Allard. The BT-Settl Model Atmospheres for Stars, Brown Dwarfs and Planets. In Mark Booth, Brenda C. Matthews, and James R. Graham, editors, *Exploring the Formation and Evolution of Planetary Systems*, volume 299, pages 271–272, January 2014. (document), 2.2, A.1

[8] Mark J. Pecaut and Eric E. Mamajek. Intrinsic Colors, Temperatures, and Bolometric Corrections of Pre-main-sequence Stars. , 208(1):9, September 2013. (document), 2.5, 2.2, 3.3.3, A.1

[9] Christopher F. McKee and Eve C. Ostriker. Theory of Star Formation. , 45(1):565–687, September 2007. 1.1

[10] E. Tognelli, P. G. Prada Moroni, and S. Degl'Innocenti. The Pisa pre-main sequence tracks and isochrones. A database covering a wide range of Z, Y, mass, and age values. , 533:A109, September 2011. 1.1

[11] Sean M. Andrews. Observations of Protoplanetary Disk Structures. , 58:483–528, August 2020. 1.1, 2.6, 3

[12] Charles J. Lada and Elizabeth A. Lada. Embedded Clusters in Molecular Clouds. , 41:57–115, January 2003. 1.2

[13] Joel H. Kastner and David A. Principe. Nearby Young Stars and Young Moving Groups. In *Handbook of X-ray and Gamma-ray Astrophysics*, page 49. 2022. 1.2

[14] Jonathan Gagné, Jacqueline K. Faherty, Leslie Moranta, and Mark Popinchalk. A Number of nearby Moving Groups May Be Fragments of Dissolving Open Clusters. , 915(2):L29, July 2021. 1.2

[15] Thomas Preibisch and Eric D. Feigelson. The Evolution of X-Ray Emission in Young Stars. , 160(2):390–400, October 2005. 1.2

[16] J. H. Kastner, B. Zuckerman, D. A. Weintraub, and T. Forveille. X-ray and molecular emission from the nearest region of recent star formation. *Science*, 277:67–71, January 1997. 1.2

[17] M. Steinmetz, T. Zwitter, A. Siebert, F. G. Watson, K. C. Freeman, U. Munari, R. Campbell, M. Williams, G. M. Seabroke, R. F. G. Wyse, Q. A. Parker, O. Bienaymé, S. Roeser, B. K. Gibson, G. Gilmore, E. K. Grebel, A. Helmi, J. F. Navarro, D. Burton, C. J. P. Cass, J. A. Dawe, K. Fiegert, M. Hartley, K. S. Russell, W. Saunders, H. Enke, J. Bailin, J. Binney, J. Bland-Hawthorn, C. Boeche, W. Dehnen, D. J. Eisenstein, N. W. Evans, M. Fiorucci, J. P. Fulbright, O. Gerhard, U. Jauregi, A. Kelz, L. Mijović, I. Minchev, G. Parmentier, J. Peñarrubia, A. C. Quillen, M. A. Read, G. Ruchti, R. D. Scholz, A. Siviero, M. C. Smith, R. Sordo, L. Veltz, S. Vidrih, R. von Berlepsch, B. J. Boyle, and E. Schilbach. The Radial Velocity Experiment (RAVE): First Data Release. , 132(4):1645–1668, October 2006. 1.2

[18] Gaia Collaboration, T. Prusti, J. H. J. de Bruijne, A. G. A. Brown, A. Vallenari, C. Babusiaux, C. A. L. Bailer-Jones, U. Bastian, M. Biermann, D. W. Evans, L. Eyer, F. Jansen, C. Jordi, S. A. Klioner, U. Lammers, L. Lindegren, X. Luri, F. Mignard, D. J. Milligan, C. Panem, V. Poinsignon, D. Pourbaix, S. Randich, G. Sarri, P. Sartoretti, H. I. Siddiqui, C. Soubiran, V. Valette, F. van Leeuwen, N. A. Walton, C. Aerts, F. Arenou, M. Cropper, R. Drimmel, E. Høg, D. Katz, M. G. Lattanzi, W. O'Mullane, E. K. Grebel, A. D. Holland, C. Huc, X. Passot, L. Bramante, C. Cacciari, J. Castañeda, L. Chaoul, N. Cheek, F. De Angeli, C. Fabricius, R. Guerra, J. Hernández, A. Jean-Antoine-Piccolo, E. Masana, R. Messineo, N. Mowlavi, K. Nienartowicz, D. Ordóñez-Blanco, P. Panuzzo, J. Portell, P. J. Richards, M. Riello, G. M. Seabroke, P. Tanga, F. Thévenin, J. Torra, S. G. Els, G. Gracia-Abril, G. Comoretto, M. Garcia-Reinaldos, T. Lock, E. Mercier, M. Altmann, R. Andrae, T. L. Astraatmadja, I. Bellas-Velidis, K. Benson, J. Berthier, R. Blomme, G. Busso, B. Carry, A. Cellino, G. Clementini, S. Cowell, O. Creevey, J. Cuypers, M. Davidson, J. De Ridder, A. de Torres, L. Delchambre, A. Dell'Oro, C. Ducourant, Y. Frémat, M. García-Torres, E. Gosset, J. L. Halbwachs, N. C. Hambly, D. L. Harrison, M. Hauser, D. Hestroffer, S. T. Hodgkin, H. E. Huckle, A. Hutton, G. Jasniewicz, S. Jordan, M. Kontizas, A. J. Korn, A. C. Lanzafame, M. Manteiga, A. Moitinho, K. Muinonen, J. Osinde, E. Pancino, T. Pauwels, J. M. Petit,

A. Recio-Blanco, A. C. Robin, L. M. Sarro, C. Siopis, M. Smith, K. W. Smith, A. Sozzetti, W. Thuillot, W. van Reeven, Y. Viala, U. Abbas, A. Abreu Aramburu, S. Accart, J. J. Aguado, P. M. Allan, W. Allasia, G. Altavilla, M. A. Álvarez, J. Alves, R. I. Anderson, A. H. Andrei, E. Anglada Varela, E. Antiche, T. Antoja, S. Antón, B. Arcay, A. Atzei, L. Ayache, N. Bach, S. G. Baker, L. Balaguer-Núñez, C. Barache, C. Barata, A. Barbier, F. Barblan, M. Baroni, D. Barrado y Navascués, M. Barros, M. A. Barstow, U. Becciani, M. Bellazzini, G. Bellei, A. Bello García, V. Belokurov, P. Bendjoya, A. Berihuete, L. Bianchi, O. Bienaymé, F. Billebaud, N. Blagorodnova, S. Blanco-Cuaresma, T. Boch, A. Bombrun, R. Borrachero, S. Bouquillon, G. Bourda, H. Bouy, A. Bragaglia, M. A. Breddels, N. Brouillet, T. Brüsemeister, B. Bucciarelli, F. Budnik, P. Burgess, R. Burgon, A. Burlacu, D. Busonero, R. Buzzi, E. Caffau, J. Cambras, H. Campbell, R. Cancelliere, T. Cantat-Gaudin, T. Carlucci, J. M. Carrasco, M. Castellani, P. Charlot, J. Charnas, P. Charvet, F. Chassat, A. Chiavassa, M. Clotet, G. Cocozza, R. S. Collins, P. Collins, G. Costigan, F. Crifo, N. J. G. Cross, M. Crosta, C. Crowley, C. Dafonte, Y. Damerdji, A. Dapergolas, P. David, M. David, P. De Cat, F. de Felice, P. de Laverny, F. De Luise, R. De March, D. de Martino, R. de Souza, J. Debosscher, E. del Pozo, M. Delbo, A. Delgado, H. E. Delgado, F. di Marco, P. Di Matteo, S. Diakite, E. Distefano, C. Dolding, S. Dos Anjos, P. Drazinos, J. Durán, Y. Dzigan, E. Ecale, B. Edvardsson, H. Enke, M. Erdmann, D. Escolar, M. Espina, N. W. Evans, G. Eynard Bontemps, C. Fabre, M. Fabrizio, S. Faigler, A. J. Falcão, M. Farràs Casas, F. Faye, L. Federici, G. Fedorets, J. Fernández-Hernández, P. Fernique, A. Fienga, F. Figueras, F. Filippi, K. Findeisen, A. Fonti, M. Fouesneau, E. Fraile, M. Fraser, J. Fuchs, R. Furnell, M. Gai, S. Galleti, L. Galluccio, D. Garabato, F. García-Sedano, P. Garé, A. Garofalo, N. Garralda, P. Gavras, J. Gerssen, R. Geyer, G. Gilmore, S. Girona, G. Giuffrida, M. Gomes, A. González-Marcos, J. González-Núñez, J. J. González-Vidal, M. Granvik, A. Guerrier, P. Guillout, J. Guiraud, A. Gúrpide, R. Gutiérrez-Sánchez, L. P. Guy, R. Haigron, D. Hatzidimitriou, M. Haywood, U. Heiter, A. Helmi, D. Hobbs, W. Hofmann, B. Holl, G. Holland, J. A. S. Hunt, A. Hypki, V. Icardi, M. Irwin, G. Jevardat de Fombelle, P. Jofré, P. G.

Jonker, A. Jorissen, F. Julbe, A. Karampelas, A. Kochoska, R. Kohley, K. Kolenberg, E. Kontizas, S. E. Koposov, G. Kordopatis, P. Koubsky, A. Kowalczyk, A. Krone-Martins, M. Kudryashova, I. Kull, R. K. Bachchan, F. Lacoste-Seris, A. F. Lanza, J. B. Lavigne, C. Le Poncin-Lafitte, Y. Lebreton, T. Lebzelter, S. Leccia, N. Leclerc, I. Lecoeur-Taibi, V. Lemaitre, H. Lenhardt, F. Leroux, S. Liao, E. Licata, H. E. P. Lindstrøm, T. A. Lister, E. Livanou, A. Lobel, W. Löffler, M. López, A. Lopez-Lozano, D. Lorenz, T. Loureiro, I. MacDonald, T. Magalhães Fernandes, S. Managau, R. G. Mann, G. Mantelet, O. Marchal, J. M. Marchant, M. Marconi, J. Marie, S. Marinoni, P. M. Marrese, G. Marschalkó, D. J. Marshall, J. M. Martín-Fleitas, M. Martino, N. Mary, G. Matijevič, T. Mazeh, P. J. McMillan, S. Messina, A. Mestre, D. Michalik, N. R. Millar, B. M. H. Miranda, D. Molina, R. Molinaro, M. Molinaro, L. Molnár, M. Moniez, P. Montegriffo, D. Monteiro, R. Mor, A. Mora, R. Morbidelli, T. Morel, S. Morgenthaler, T. Morley, D. Morris, A. F. Mulone, T. Muraveva, I. Musella, J. Narbonne, G. Nelemans, L. Nicastro, L. Noval, C. Ordénovic, J. Ordieres-Meré, P. Osborne, C. Pagani, I. Pagano, F. Pailler, H. Palacin, L. Palaversa, P. Parsons, T. Paulsen, M. Pecoraro, R. Pedrosa, H. Pentikäinen, J. Pereira, B. Pichon, A. M. Piersimoni, F. X. Pineau, E. Plachy, G. Plum, E. Poujoulet, A. Prša, L. Pulone, S. Ragaini, S. Rago, N. Rambaux, M. Ramos-Lerate, P. Ranalli, G. Rauw, A. Read, S. Regibo, F. Renk, C. Reylé, R. A. Ribeiro, L. Rimoldini, V. Ripepi, A. Riva, G. Rixon, M. Roelens, M. Romero-Gómez, N. Rowell, F. Royer, A. Rudolph, L. Ruiz-Dern, G. Sadowski, T. Sagristà Sellés, J. Sahlmann, J. Salgado, E. Salguero, M. Sarasso, H. Savietto, A. Schnorhk, M. Schultheis, E. Sciacca, M. Segol, J. C. Segovia, D. Segransan, E. Serpell, I. C. Shih, R. Smareglia, R. L. Smart, C. Smith, E. Solano, F. Solitro, R. Sordo, S. Soria Nieto, J. Souchay, A. Spagna, F. Spoto, U. Stampa, I. A. Steele, H. Steidelmüller, C. A. Stephenson, H. Stoev, F. F. Suess, M. Süveges, J. Surdej, L. Szabados, E. Szegedi-Elek, D. Tapiador, F. Taris, G. Tauran, M. B. Taylor, R. Teixeira, D. Terrett, B. Tingley, S. C. Trager, C. Turon, A. Ulla, E. Utrilla, G. Valentini, A. van Elteren, E. Van Hemelryck, M. van Leeuwen, M. Varadi, A. Vecchiato, J. Veljanoski, T. Via, D. Vicente, S. Vogt, H. Voss, V. Votruba, S. Voutsinas, G. Walmsley, M. Weiler, K. Weingrill, D. Werner,

T. Wevers, G. Whitehead, Ł. Wyrzykowski, A. Yoldas, M. Žerjal, S. Zucker, C. Zurbach, T. Zwitter, A. Alecu, M. Allen, C. Allende Prieto, A. Amorim, G. Anglada-Escudé, V. Arsenijevic, S. Azaz, P. Balm, M. Beck, H. H. Bernstein, L. Bigot, A. Bijaoui, C. Blasco, M. Bonfigli, G. Bono, S. Boudreault, A. Bressan, S. Brown, P. M. Brunet, P. Bunclark, R. Buonanno, A. G. Butkevich, C. Carret, C. Carrion, L. Chemin, F. Chéreau, L. Corcione, E. Darmigny, K. S. de Boer, P. de Teodoro, P. T. de Zeeuw, C. Delle Luche, C. D. Domingues, P. Dubath, F. Fodor, B. Frézouls, A. Fries, D. Fustes, D. Fyfe, E. Gallardo, J. Gallegos, D. Gardiol, M. Gebran, A. Gomboc, A. Gómez, E. Grux, A. Gueguen, A. Heyrovsky, J. Hoar, G. Iannicola, Y. Isasi Parache, A. M. Janotto, E. Joliet, A. Jonckheere, R. Keil, D. W. Kim, P. Klagyivik, J. Klar, J. Knude, O. Kochukhov, I. Kolka, J. Kos, A. Kutka, V. Lainey, D. LeBouquin, C. Liu, D. Loreggia, V. V. Makarov, M. G. Marseille, C. Martayan, O. Martinez-Rubi, B. Massart, F. Meynadier, S. Mignot, U. Munari, A. T. Nguyen, T. Nordlander, P. Ocvirk, K. S. O'Flaherty, A. Olias Sanz, P. Ortiz, J. Osorio, D. Oszkiewicz, A. Ouzounis, M. Palmer, P. Park, E. Pasquato, C. Peltzer, J. Peralta, F. Péturaud, T. Pieniluoma, E. Pigozzi, J. Poels, G. Prat, T. Prod'homme, F. Raison, J. M. Rebordao, D. Risquez, B. Rocca-Volmerange, S. Rosen, M. I. Ruiz-Fuertes, F. Russo, S. Sembay, I. Serraller Vizcaino, A. Short, A. Siebert, H. Silva, D. Sinachopoulos, E. Slezak, M. Soffel, D. Sosnowska, V. Straižys, M. ter Linden, D. Terrell, S. Theil, C. Tiede, L. Troisi, P. Tsalmantza, D. Tur, M. Vaccari, F. Vachier, P. Valles, W. Van Hamme, L. Veltz, J. Virtanen, J. M. Wallut, R. Wichmann, M. I. Wilkinson, H. Ziaeepour, and S. Zschocke. The Gaia mission. , 595:A1, November 2016. 1.2, 1.4

[19] David A. Weintraub, Tracy Huard, Joel H. Kastner, and Ian Gatley. The Onset of Molecular Hydrogen Emission from Proto-planetary Nebulae. , 509(2):728–732, December 1998. 1.3

[20] E. C. Wilson and J. Nordhaus. Convection and spin-up during common envelope evolution: the formation of short-period double white dwarfs. , 497(2):1895–1903, September 2020. 1.3

[21] M. F. Sousa, J. G. Coelho, J. C. N. de Araujo, S. O. Kepler, and J. A. Rueda. The Double White Dwarf Merger Progenitors of SDSS J2211+1136 and ZTF J1901+1458. , 941(1):28, December 2022. 1.3

[22] Gaia Collaboration, A. Vallenari, A. G. A. Brown, T. Prusti, J. H. J. de Bruijne, F. Arenou, C. Babusiaux, M. Biermann, O. L. Creevey, C. Ducourant, D. W. Evans, L. Eyer, R. Guerra, A. Hutton, C. Jordi, S. A. Klioner, U. L. Lammers, L. Lindegren, X. Luri, F. Mignard, C. Panem, D. Pourbaix, S. Randich, P. Sartoretti, C. Soubiran, P. Tanga, N. A. Walton, C. A. L. Bailer-Jones, U. Bastian, R. Drimmel, F. Jansen, D. Katz, M. G. Lattanzi, F. van Leeuwen, J. Bakker, C. Cacciari, J. Castañeda, F. De Angeli, C. Fabricius, M. Fouesneau, Y. Frémat, L. Galluccio, A. Guerrier, U. Heiter, E. Masana, R. Messineo, N. Mowlavi, C. Nicolas, K. Nienartowicz, F. Pailler, P. Panuzzo, F. Riclet, W. Roux, G. M. Seabroke, R. Sordo, F. Thévenin, G. Gracia-Abril, J. Portell, D. Teyssier, M. Altmann, R. Andrae, M. Audard, I. Bellas-Velidis, K. Benson, J. Berthier, R. Blomme, P. W. Burgess, D. Busonero, G. Busso, H. Cánovas, B. Carry, A. Cellino, N. Cheek, G. Clementini, Y. Damerdji, M. Davidson, P. de Teodoro, M. Nuñez Campos, L. Delchambre, A. Dell'Oro, P. Esquej, J. Fernández-Hernández, E. Fraile, D. Garabato, P. García-Lario, E. Gosset, R. Haigron, J. L. Halbwachs, N. C. Hambly, D. L. Harrison, J. Hernández, D. Hestroffer, S. T. Hodgkin, B. Holl, K. Janßen, G. Jevardat de Fombelle, S. Jordan, A. Krone-Martins, A. C. Lanzafame, W. Löffler, O. Marchal, P. M. Marrese, A. Moitinho, K. Muinonen, P. Osborne, E. Pancino, T. Pauwels, A. Recio-Blanco, C. Reylé, M. Riello, L. Rimoldini, T. Roegiers, J. Rybizki, L. M. Sarro, C. Siopis, M. Smith, A. Sozzetti, E. Utrilla, M. van Leeuwen, U. Abbas, P. Ábrahám, A. Abreu Aramburu, C. Aerts, J. J. Aguado, M. Ajaj, F. Aldea-Montero, G. Altavilla, M. A. Álvarez, J. Alves, F. Anders, R. I. Anderson, E. Anglada Varela, T. Antoja, D. Baines, S. G. Baker, L. Balaguer-Núñez, E. Balbinot, Z. Balog, C. Barache, D. Barbato, M. Barros, M. A. Barstow, S. Bartolomé, J. L. Bassilana, N. Bauchet, U. Becciani, M. Bellazzini, A. Berihuete, M. Bernet, S. Bertone, L. Bianchi, A. Binnenfeld, S. Blanco-Cuaresma, A. Blazere, T. Boch, A. Bombrun, D. Bossini, S. Bouquillon, A. Bragaglia, L. Bramante, E. Breedt, A. Bres-

san, N. Brouillet, E. Brugaletta, B. Bucciarelli, A. Burlacu, A. G. Butkevich, R. Buzzi, E. Caffau, R. Cancelliere, T. Cantat-Gaudin, R. Carballo, T. Carlucci, M. I. Carnerero, J. M. Carrasco, L. Casamiquela, M. Castellani, A. Castro-Ginard, L. Chaoul, P. Charlot, L. Chemin, V. Chiaramida, A. Chiavassa, N. Chornay, G. Comoretto, G. Contursi, W. J. Cooper, T. Cornez, S. Cowell, F. Crifo, M. Cropper, M. Crosta, C. Crowley, C. Dafonte, A. Dapergolas, M. David, P. David, P. de Laverny, F. De Luise, R. De March, J. De Ridder, R. de Souza, A. de Torres, E. F. del Peloso, E. del Pozo, M. Delbo, A. Delgado, J. B. Delisle, C. Demouchy, T. E. Dharmawardena, P. Di Matteo, S. Diakite, C. Diener, E. Distefano, C. Dolding, B. Edvardsson, H. Enke, C. Fabre, M. Fabrizio, S. Faigler, G. Fedorets, P. Fernique, A. Fienga, F. Figueras, Y. Fournier, C. Fouron, F. Fragkoudi, M. Gai, A. Garcia-Gutierrez, M. Garcia-Reinaldos, M. García-Torres, A. Garofalo, A. Gavel, P. Gavras, E. Gerlach, R. Geyer, P. Giacobbe, G. Gilmore, S. Girona, G. Giuffrida, R. Gomel, A. Gomez, J. González-Núñez, I. González-Santamaría, J. J. González-Vidal, M. Granvik, P. Guillout, J. Guiraud, R. Gutiérrez-Sánchez, L. P. Guy, D. Hatzidimitriou, M. Hauser, M. Haywood, A. Helmer, A. Helmi, M. H. Sarmiento, S. L. Hidalgo, T. Hilger, N. Hładczuk, D. Hobbs, G. Holland, H. E. Huckle, K. Jardine, G. Jasniewicz, A. Jean-Antoine Piccolo, Ó. Jiménez-Arranz, A. Jorissen, J. Juaristi Campillo, F. Julbe, L. Karbevska, P. Kervella, S. Khanna, M. Kontizas, G. Kordopatis, A. J. Korn, Á. Kóspál, Z. Kostrzewa-Rutkowska, K. Kruszyńska, M. Kun, P. Laizeau, S. Lambert, A. F. Lanza, Y. Lasne, J. F. Le Campion, Y. Lebreton, T. Lebzelter, S. Leccia, N. Leclerc, I. Lecoeur-Taibi, S. Liao, E. L. Licata, H. E. P. Lindstrøm, T. A. Lister, E. Livanou, A. Lobel, A. Lorca, C. Loup, P. Madrero Pardo, A. Magdaleno Romeo, S. Managau, R. G. Mann, M. Manteiga, J. M. Marchant, M. Marconi, J. Marcos, M. M. S. Marcos Santos, D. Marín Pina, S. Marinoni, F. Marocco, D. J. Marshall, L. Martin Polo, J. M. Martín-Fleitas, G. Marton, N. Mary, A. Masip, D. Massari, A. Mastrobuono-Battisti, T. Mazeh, P. J. McMillan, S. Messina, D. Michalik, N. R. Millar, A. Mints, D. Molina, R. Molinaro, L. Molnár, G. Monari, M. Monguió, P. Montegriffo, A. Montero, R. Mor, A. Mora, R. Morbidelli, T. Morel, D. Morris, T. Muraveva, C. P. Murphy, I. Musella, Z. Nagy, L. Noval,

F. Ocaña, A. Ogden, C. Ordenovic, J. O. Osinde, C. Pagani, I. Pagano, L. Palaversa, P. A. Palicio, L. Pallas-Quintela, A. Panahi, S. Payne-Wardenaar, X. Peñalosa Esteller, A. Penttilä, B. Pichon, A. M. Piersimoni, F. X. Pineau, E. Plachy, G. Plum, E. Poggio, A. Prša, L. Pulone, E. Racero, S. Ragaini, M. Rainer, C. M. Raiteri, N. Rambaux, P. Ramos, M. Ramos-Lerate, P. Re Fiorentin, S. Regibo, P. J. Richards, C. Rios Diaz, V. Ripepi, A. Riva, H. W. Rix, G. Rixon, N. Robichon, A. C. Robin, C. Robin, M. Roelens, H. R. O. Rogues, L. Rohrbasser, M. Romero-Gómez, N. Rowell, F. Royer, D. Ruz Mieres, K. A. Rybicki, G. Sadowski, A. Sáez Núñez, A. Sagristà Sellés, J. Sahlmann, E. Salguero, N. Samaras, V. Sanchez Gimenez, N. Sanna, R. Santoveña, M. Sarasso, M. Schultheis, E. Sciacca, M. Segol, J. C. Segovia, D. Ségransan, D. Semeux, S. Shahaf, H. I. Siddiqui, A. Siebert, L. Siltala, A. Silvelo, E. Slezak, I. Slezak, R. L. Smart, O. N. Snaith, E. Solano, F. Solitro, D. Souami, J. Souchay, A. Spagna, L. Spina, F. Spoto, I. A. Steele, H. Steidelmüller, C. A. Stephenson, M. Süveges, J. Surdej, L. Szabados, E. Szegedi-Elek, F. Taris, M. B. Taylor, R. Teixeira, L. Tolomei, N. Tonello, F. Torra, J. Torra, G. Torralba Elipe, M. Trabucchi, A. T. Tsounis, C. Turon, A. Ulla, N. Unger, M. V. Vaillant, E. van Dillen, W. van Reeven, O. Vanel, A. Vecchiato, Y. Viala, D. Vicente, S. Voutsinas, M. Weiler, T. Wevers, Ł. Wyrzykowski, A. Yoldas, P. Yvard, H. Zhao, J. Zorec, S. Zucker, and T. Zwitter. Gaia Data Release 3. Summary of the content and survey properties. , 674:A1, June 2023. 1.4

[23] T. H. Jarrett, A. Comrie, L. Marchetti, A. Sivitilli, S. Macfarlane, F. Vitello, U. Becciani, A. R. Taylor, J. M. van der Hulst, P. Serra, N. Katz, and M. E. Cluver. Exploring and interrogating astrophysical data in virtual reality. *Astronomy and Computing*, 37:100502, October 2021. 1.5

[24] C. Impey and A. Danehy. Exploring the Frontiers of Space in 3D: Immersive Virtual Reality for Astronomy Outreach. *Communicating Astronomy with the Public Journal*, 31:28, October 2022. 1.5

[25] Lucia Marchetti, Thomas H. Jarrett, Angus Comrie, Alexander K. Sivitilli, Fabio Vitello,

Ugo Becciani, and A. R. Taylor. iDaVIE-v: immersive Data Visualisation Interactive Explorer for volumetric rendering. *arXiv e-prints*, page arXiv:2012.11553, December 2020. 1.5

[26] Antoni Sagristà, Stefan Jordan, Thomas Müller, and Filip Sadlo. Gaia sky: Navigating the gaia catalog. *IEEE Transactions on Visualization and Computer Graphics*, 25(1):1070–1079, 2019. 1.5

[27] Susan Higashio, Marc J. Kuchner, Steven M. Silverberg, Matthew A. Brandt, Thomas G. Grubb, Jonathan Gagné, John H. Debes, Joshua Schlieder, John P. Wisniewski, Stewart Slocum, Alissa S. Bans, Shambo Bhattacharjee, Joseph R. Biggs, Milton K. D. Bosch, Tadeas Cernohous, Katharina Doll, Hugo A. Durantini Luca, Alexandru Enachioaie, Phillip Griffith, Joshua Hamilton, Jonathan Holden, Michiharu Hyogo, Dawoon Jung, Lily Lau, Fernanda Piñeiro, Art Piipuu, Lisa Stiller, and Disk Detective Collaboration. Disks in Nearby Young Stellar Associations Found Via Virtual Reality. , 933(1):13, July 2022. 1.5, 5.2

[28] C. J. Fluke and D. G. Barnes. Immersive Virtual Reality Experiences for All-Sky Data. , 35:e026, June 2018. 1.5

[29] M. B. Taylor. TOPCAT & STIL: Starlink Table/VOTable Processing Software. In P. Shopbell, M. Britton, and R. Ebert, editors, *Astronomical Data Analysis Software and Systems XIV*, volume 347 of *Astronomical Society of the Pacific Conference Series*, page 29, December 2005. 1.5

[30] Dalya Baron. Machine Learning in Astronomy: a practical overview. *arXiv e-prints*, page arXiv:1904.07248, April 2019. 2.1.1

[31] Gaia Collaboration, A. G. A. Brown, A. Vallenari, T. Prusti, J. H. J. de Bruijne, C. Babusiaux, M. Biermann, O. L. Creevey, D. W. Evans, L. Eyer, A. Hutton, F. Jansen, C. Jordi, S. A. Klioner, U. Lammers, L. Lindegren, X. Luri, F. Mignard, C. Panem, D. Pourbaix, S. Randich, P. Sartoretti, C. Soubiran, N. A. Walton, F. Arenou, C. A. L. Bailer-Jones,

U. Bastian, M. Cropper, R. Drimmel, D. Katz, M. G. Lattanzi, F. van Leeuwen, J. Bakker, C. Cacciari, J. Castañeda, F. De Angeli, C. Ducourant, C. Fabricius, M. Fouesneau, Y. Frémat, R. Guerra, A. Guerrier, J. Guiraud, A. Jean-Antoine Piccolo, E. Masana, R. Messineo, N. Mowlavi, C. Nicolas, K. Nienartowicz, F. Pailler, P. Panuzzo, F. Riclet, W. Roux, G. M. Seabroke, R. Sordo, P. Tanga, F. Thévenin, G. Gracia-Abril, J. Portell, D. Teyssier, M. Altmann, R. Andrae, I. Bellas-Velidis, K. Benson, J. Berthier, R. Blomme, E. Brugaletta, P. W. Burgess, G. Busso, B. Carry, A. Cellino, N. Cheek, G. Clementini, Y. Damerdji, M. Davidson, L. Delchambre, A. Dell'Oro, J. Fernández-Hernández, L. Galluccio, P. García-Lario, M. Garcia-Reinaldos, J. González-Núñez, E. Gosset, R. Haigron, J. L. Halbwachs, N. C. Hambly, D. L. Harrison, D. Hatzidimitriou, U. Heiter, J. Hernández, D. Hestroffer, S. T. Hodgkin, B. Holl, K. Janßen, G. Jevardat de Fombelle, S. Jordan, A. Krone-Martins, A. C. Lanzafame, W. Löffler, A. Lorca, M. Manteiga, O. Marchal, P. M. Marrese, A. Moitinho, A. Mora, K. Muinonen, P. Osborne, E. Pancino, T. Pauwels, J. M. Petit, A. Recio-Blanco, P. J. Richards, M. Riello, L. Rimoldini, A. C. Robin, T. Roegiers, J. Rybizki, L. M. Sarro, C. Siopis, M. Smith, A. Sozzetti, A. Ulla, E. Utrilla, M. van Leeuwen, W. van Reeven, U. Abbas, A. Abreu Aramburu, S. Accart, C. Aerts, J. J. Aguado, M. Ajaj, G. Altavilla, M. A. Álvarez, J. Álvarez Cid-Fuentes, J. Alves, R. I. Anderson, E. Anglada Varela, T. Antoja, M. Audard, D. Baines, S. G. Baker, L. Balaguer-Núñez, E. Balbinot, Z. Balog, C. Barache, D. Barbato, M. Barros, M. A. Barstow, S. Bartolomé, J. L. Bassilana, N. Bauchet, A. Baudesson-Stella, U. Becciani, M. Bellazzini, M. Bernet, S. Bertone, L. Bianchi, S. Blanco-Cuaresma, T. Boch, A. Bombrun, D. Bossini, S. Bouquillon, A. Bragaglia, L. Bramante, E. Breedt, A. Bressan, N. Brouillet, B. Bucciarelli, A. Burlacu, D. Busonero, A. G. Butkevich, R. Buzzi, E. Caffau, R. Cancelliere, H. Cánovas, T. Cantat-Gaudin, R. Carballo, T. Carlucci, M. I. Carnerero, J. M. Carrasco, L. Casamiquela, M. Castellani, A. Castro-Ginard, P. Castro Sampol, L. Chaoul, P. Charlot, L. Chemin, A. Chiavassa, M. R. L. Cioni, G. Comoretto, W. J. Cooper, T. Cornez, S. Cowell, F. Crifo, M. Crosta, C. Crowley, C. Dafonte, A. Dapergolas, M. David, P. David, P. de Laverny, F. De Luise, R. De March, J. De Ridder, R. de Souza, P. de

Teodoro, A. de Torres, E. F. del Peloso, E. del Pozo, M. Delbo, A. Delgado, H. E. Delgado, J. B. Delisle, P. Di Matteo, S. Diakite, C. Diener, E. Distefano, C. Dolding, D. Eappachen, B. Edvardsson, H. Enke, P. Esquej, C. Fabre, M. Fabrizio, S. Faigler, G. Fedorets, P. Fernique, A. Fienga, F. Figueras, C. Fouron, F. Fragkoudi, E. Fraile, F. Franke, M. Gai, D. Garabato, A. Garcia-Gutierrez, M. García-Torres, A. Garofalo, P. Gavras, E. Gerlach, R. Geyer, P. Giacobbe, G. Gilmore, S. Girona, G. Giuffrida, R. Gomel, A. Gomez, I. Gonzalez-Santamaria, J. J. González-Vidal, M. Granvik, R. Gutiérrez-Sánchez, L. P. Guy, M. Hauser, M. Haywood, A. Helmi, S. L. Hidalgo, T. Hilger, N. Hładczuk, D. Hobbs, G. Holland, H. E. Huckle, G. Jasniewicz, P. G. Jonker, J. Juaristi Campillo, F. Julbe, L. Karbevska, P. Kervella, S. Khanna, A. Kochoska, M. Kontizas, G. Kordopatis, A. J. Korn, Z. Kostrzewa-Rutkowska, K. Kruszyńska, S. Lambert, A. F. Lanza, Y. Lasne, J. F. Le Campion, Y. Le Fustec, Y. Lebreton, T. Lebzelter, S. Leccia, N. Leclerc, I. Lecoeur-Taibi, S. Liao, E. Licata, E. P. Lindstrøm, T. A. Lister, E. Livanou, A. Lobel, P. Madrero Pardo, S. Managau, R. G. Mann, J. M. Marchant, M. Marconi, M. M. S. Marcos Santos, S. Marinoni, F. Marocco, D. J. Marshall, L. Martin Polo, J. M. Martín-Fleitas, A. Masip, D. Massari, A. Mastrobuono-Battisti, T. Mazeh, P. J. McMillan, S. Messina, D. Michalik, N. R. Millar, A. Mints, D. Molina, R. Molinaro, L. Molnár, P. Montegriffo, R. Mor, R. Morbidelli, T. Morel, D. Morris, A. F. Mulone, D. Munoz, T. Muraveva, C. P. Murphy, I. Musella, L. Noval, C. Ordénovic, G. Orrù, J. Osinde, C. Pagani, I. Pagano, L. Palaversa, P. A. Palicio, A. Panahi, M. Pawlak, X. Peñalosa Esteller, A. Penttilä, A. M. Piersimoni, F. X. Pineau, E. Plachy, G. Plum, E. Poggio, E. Poretti, E. Poujoulet, A. Prša, L. Pulone, E. Racero, S. Ragaini, M. Rainer, C. M. Raiteri, N. Rambaux, P. Ramos, M. Ramos-Lerate, P. Re Fiorentin, S. Regibo, C. Reylé, V. Ripepi, A. Riva, G. Rixon, N. Robichon, C. Robin, M. Roelens, L. Rohrbasser, M. Romero-Gómez, N. Rowell, F. Royer, K. A. Rybicki, G. Sadowski, A. Sagristà Sellés, J. Sahlmann, J. Salgado, E. Salguero, N. Samaras, V. Sanchez Gimenez, N. Sanna, R. Santoveña, M. Sarasso, M. Schultheis, E. Sciacca, M. Segol, J. C. Segovia, D. Ségransan, D. Semeux, S. Shahaf, H. I. Siddiqui, A. Siebert, L. Siltala, E. Slezak, R. L. Smart, E. Solano, F. Solitro, D. Souami, J. Souchay,

A. Spagna, F. Spoto, I. A. Steele, H. Steidelmüller, C. A. Stephenson, M. Süveges, L. Szabados, E. Szegedi-Elek, F. Taris, G. Tauran, M. B. Taylor, R. Teixeira, W. Thuillot, N. Tonello, F. Torra, J. Torra, C. Turon, N. Unger, M. Vaillant, E. van Dillen, O. Vanel, A. Vecchiato, Y. Viala, D. Vicente, S. Voutsinas, M. Weiler, T. Wevers, Ł. Wyrzykowski, A. Yoldas, P. Yvard, H. Zhao, J. Zorec, S. Zucker, C. Zurbach, and T. Zwitter. Gaia Early Data Release 3. Summary of the contents and survey properties. , 649:A1, May 2021. 2.2.1

[32] W. B. Landsman. The IDL Astronomy User's Library. In R. J. Hanisch, R. J. V. Brissenden, and J. Barnes, editors, *Astronomical Data Analysis Software and Systems II*, volume 52 of *Astronomical Society of the Pacific Conference Series*, page 246, January 1993. 2.2.2.1

[33] M. Cropper, D. Katz, P. Sartoretti, T. Prusti, J. H. J. de Bruijne, F. Chassat, P. Charvet, J. Boyadjian, M. Perryman, G. Sarri, P. Gare, M. Erdmann, U. Munari, T. Zwitter, M. Wilkinson, F. Arenou, A. Vallenari, A. Gómez, P. Panuzzo, G. Seabroke, C. Allende Prieto, K. Benson, O. Marchal, H. Huckle, M. Smith, C. Dolding, K. Janßen, Y. Viala, R. Blomme, S. Baker, S. Boudreault, F. Crifo, C. Soubiran, Y. Frémat, G. Jasniewicz, A. Guerrier, L. P. Guy, C. Turon, A. Jean-Antoine-Piccolo, F. Thévenin, M. David, E. Gosset, and Y. Damerdji. Gaia Data Release 2. Gaia Radial Velocity Spectrometer. , 616:A5, August 2018. 2.2.2.1, 3.4

[34] M. Wenger, F. Ochsenbein, D. Egret, P. Dubois, F. Bonnarel, S. Borde, F. Genova, G. Jasniewicz, S. Laloë, S. Lesteven, and R. Monier. The SIMBAD astronomical database. The CDS reference database for astronomical objects. , 143:9–22, April 2000. 2.3

[35] Ochsenbein F. et. al. The VizieR database of astronomical catalogues . 2.3

[36] K. L. Luhman, John R. Stauffer, and E. E. Mamajek. The Age of AB Doradus. , 628(1):L69–L72, July 2005. 2.3, 4.1

[37] Ronan Kerr, Adam L. Kraus, Simon J. Murphy, Daniel M. Krolikowski, Timothy R. Bedding, and Aaron C. Rizzuto. SPYGLASS. III. The Fornax-Horologium Association and Its Traceback History within the Austral Complex. , 941(2):143, December 2022. 2.3

[38] D. Christopher Martin, James Fanson, David Schiminovich, Patrick Morrissey, Peter G. Friedman, Tom A. Barlow, Tim Conrow, Robert Grange, Patrick N. Jelinsky, Bruno Milliard, Oswald H. W. Siegmund, Luciana Bianchi, Yong-Ik Byun, Jose Donas, Karl Forster, Timothy M. Heckman, Young-Wook Lee, Barry F. Madore, Roger F. Malina, Susan G. Neff, R. Michael Rich, Todd Small, Frank Surber, Alex S. Szalay, Barry Welsh, and Ted K. Wyder. The Galaxy Evolution Explorer: A Space Ultraviolet Survey Mission. , 619(1):L1–L6, January 2005. 2.5

[39] M. F. Skrutskie, R. M. Cutri, R. Stiening, M. D. Weinberg, S. Schneider, J. M. Carpenter, C. Beichman, R. Capps, T. Chester, J. Elias, J. Huchra, J. Liebert, C. Lonsdale, D. G. Monet, S. Price, P. Seitzer, T. Jarrett, J. D. Kirkpatrick, J. E. Gizis, E. Howard, T. Evans, J. Fowler, L. Fullmer, R. Hurt, R. Light, E. L. Kopan, K. A. Marsh, H. L. McCallon, R. Tam, S. Van Dyk, and S. Wheelock. The Two Micron All Sky Survey (2MASS). , 131(2):1163–1183, February 2006. 2.5

[40] Edward L. Wright, Peter R. M. Eisenhardt, Amy K. Mainzer, Michael E. Ressler, Roc M. Cutri, Thomas Jarrett, J. Davy Kirkpatrick, Deborah Padgett, Robert S. McMillan, Michael Skrutskie, S. A. Stanford, Martin Cohen, Russell G. Walker, John C. Mather, David Leisawitz, III Gautier, Thomas N., Ian McLean, Dominic Benford, Carol J. Lonsdale, Andrew Blain, Bryan Mendez, William R. Irace, Valerie Duval, Fengchuan Liu, Don Royer, Ingolf Heinrichsen, Joan Howard, Mark Shannon, Martha Kendall, Amy L. Walsh, Mark Larsen, Joel G. Cardon, Scott Schick, Mark Schwalm, Mohamed Abid, Beth Fabinsky, Larry Naes, and Chao-Wei Tsai. The Wide-field Infrared Survey Explorer (WISE): Mission Description and Initial On-orbit Performance. , 140(6):1868–1881, December 2010. 2.5

[41] A. Bayo, C. Rodrigo, D. Barrado Y Navascués, E. Solano, R. Gutiérrez, M. Morales-Calderón, and F. Allard. VOSA: virtual observatory SED analyzer. An application to the Collinder 69 open cluster. , 492(1):277–287, December 2008. 2.5

[42] Marc J. Kuchner, Steven M. Silverberg, Alissa S. Bans, Shambo Bhattacharjee, Scott J. Kenyon, John H. Debes, Thayne Currie, Luciano García, Dawoon Jung, Chris Lintott, Michael McElwain, Deborah L. Padgett, Luisa M. Rebull, John P. Wisniewski, Erika Nesvold, Kevin Schawinski, Michelle L. Thaller, Carol A. Grady, Joseph Biggs, Milton Bosch, Tadeáš Černohous, Hugo A. Durantini Luca, Michiharu Hyogo, Lily Lau Wan Wah, Art Piipuu, Fernanda Piñeiro, and Disk Detective Collaboration. Disk Detective: Discovery of New Circumstellar Disk Candidates through Citizen Science. , 830(2):84, October 2016. 2.6

[43] Adam Schneider, Inseok Song, Carl Melis, B. Zuckerman, Mike Bessell, Tara Hufford, and Sasha Hinkley. The Nearby, Young, Isolated, Dusty Star HD 166191. , 777(1):78, November 2013. 2.6

[44] Rahul I. Patel, Stanimir A. Metchev, and Aren Heinze. A Sensitive Identification of Warm Debris Disks in the Solar Neighborhood through Precise Calibration of Saturated WISE Photometry. , 212(1):10, May 2014. 2.6

[45] Steven M. Silverberg, John P. Wisniewski, Marc J. Kuchner, Kellen D. Lawson, Alissa S. Bans, John H. Debes, Joseph R. Biggs, Milton K. D. Bosch, Katharina Doll, Hugo A. Durantini Luca, Alexandru Enachioaie, Joshua Hamilton, Jonathan Holden, and Michiharu Hyogo. Peter Pan Disks: Long-lived Accretion Disks Around Young M Stars. , 890(2):106, February 2020. 3

[46] Stefan Laos, John P. Wisniewski, Marc J. Kuchner, Steven M. Silverberg, Hans Moritz Günther, David A. Principe, Brett Bonine, Marina Kounkel, and The Disk Detective Collaboration. Chandra Observations of Six Peter Pan Disks: Diversity of X-Ray-driven Internal Photoevaporation Rates Does Not Explain Their Rare Longevity. , 935(2):111, August 2022. 3

[47] David R. Rodriguez, Joel H. Kastner, David Wilner, and Chunhua Qi. Imaging the Molecular Disk Orbiting the Twin Young Suns of V4046 Sgr. , 720(2):1684–1690, September 2010. 3

[48] K. M. Punzi, J. H. Kastner, C. Melis, B. Zuckerman, C. Pilachowski, L. Gingerich, and T. Knapp. Is the Young Star RZ Piscium Consuming Its Own (Planetary) Offspring? , 155(1):33, January 2018. 3

[49] Brent Miszalski and Joanna Mikołajewska. Identification of new Galactic symbiotic stars with SALT - I. Initial discoveries and other emission line objects. , 440(2):1410–1419, May 2014. 3.1

[50] Quentin A. Parker, S. Phillipps, M. J. Pierce, M. Hartley, N. C. Hambly, M. A. Read, H. T. MacGillivray, S. B. Tritton, C. P. Cass, R. D. Cannon, M. Cohen, J. E. Drew, D. J. Frew, E. Hopewell, S. Mader, D. F. Malin, M. R. W. Masheder, D. H. Morgan, R. A. H. Morris, D. Russeil, K. S. Russell, and R. N. F. Walker. The AAO/UKST SuperCOSMOS Hα survey. , 362(2):689–710, September 2005. 3.1

[51] Eric E. Mamajek and Cameron P. M. Bell. On the age of the β Pictoris moving group. , 445(3):2169–2180, December 2014. 3.2

[52] N. Miret-Roig, P. A. B. Galli, W. Brandner, H. Bouy, D. Barrado, J. Olivares, T. Antoja, M. Romero-Gómez, F. Figueras, and J. Lillo-Box. Dynamical traceback age of the β Pictoris moving group. , 642:A179, October 2020. 3.2

[53] A. S. Binks and R. D. Jeffries. A lithium depletion boundary age of 21 Myr for the Beta Pictoris moving group. , 438(1):L11–L15, February 2014. 3.4

[54] F. J. Galindo-Guil, D. Barrado, H. Bouy, J. Olivares, A. Bayo, M. Morales-Calderón, N. Huélamo, L. M. Sarro, P. Rivière-Marichalar, H. Stoev, B. Montesinos, and J. R. Stauffer. Lithium depletion boundary, stellar associations, and Gaia. , 664:A70, August 2022. 3.4

[55] Mackenna Wood. *Lithium Depletion Boundary Ages of Young Planet-Hosting Stellar Associations*. PhD thesis, Chapel Hill, NC, 2023. 3.4

[56] Cameron P. M. Bell, Eric E. Mamajek, and Tim Naylor. The Isochronal Age Scale of Young Moving Groups in the Solar Neighbourhood. In J. H. Kastner, B. Stelzer, and S. A. Metchev, editors, *Young Stars & Planets Near the Sun*, volume 314, pages 41–48, January 2016. 3.4

[57] Jordi Isern. The Star Formation History in the Solar Neighborhood as Told by Massive White Dwarfs. , 878(1):L11, June 2019. 4.1

[58] M. Salaris and L. R. Bedin. A Gaia DR2 view of white dwarfs in the Hyades. , 480(3):3170–3176, November 2018. 4.1

[59] Jeremy Heyl, Ilaria Caiazzo, and Harvey B. Richer. Reconstructing the Pleiades with Gaia EDR3. , 926(2):132, February 2022. 4.1

[60] Jonathan Gagné, Gilles Fontaine, Amélie Simon, and Jacqueline K. Faherty. A Young Ultramassive White Dwarf in the AB Doradus Moving Group. , 861(2):L13, July 2018. 4.1

[61] O. J. Eggen. Degenerate Stars in the Hyades Supercluster. , 106:642, August 1993. 4.4

[62] Siegfried Röser and Elena Schilbach. A census of the nearby Pisces-Eridanus stellar stream. Commonalities with and disparities from the Pleiades. , 638:A9, June 2020. 5.2

[63] Mark J. Pecaut, Eric E. Mamajek, and Eric J. Bubar. A Revised Age for Upper Scorpius and the Star Formation History among the F-type Members of the Scorpius-Centaurus OB Association. , 746(2):154, February 2012. A.1